Expanded Genome and Proteome Reallocation in a Novel, Robust *Bacillus coagulans* Capable of Utilizing Pentose and Hexose Sugars

David Dooley[1], Seunghyun Ryu[1,] Richard J. Giannone[3], Jackson Edwards[2], Bruce S. Dien[2], Patricia J. Slininger, Cong T. Trinh[1,*]

[1]Department of Chemical and Biomolecular Engineering, University of Tennessee Knoxville

[2]United States Department of Agriculture (USDA), Agricultural Research Service (ARS), National Center for Agricultural Utilization Research (NCAUR), Bioenergy Research Unit, 1815 North University Street, Peoria, IL 61604, USA

[3]Biosciences Division, Oak Ridge National Laboratory, Oak Ridge, TN 37831

*Corresponding author. Email: ctrinh@utk.edu

ABSTRACT

Bacillus coagulans, a Gram-positive thermophilic bacterium, is recognized for its probiotic properties and recent development as a microbial cell factory. Despite its importance for biotechnological applications, the current understanding of *B. coagulans*' robustness is limited, especially for undomesticated strains. To fill this knowledge gap, we characterized the metabolic capability and performed functional genomics and systems analysis of a novel, robust strain, *B. coagulans* B-768. Genome sequencing revealed that B-768 has the largest *B. coagulans* genome known to date (3.94 Mbp), about 0.63 Mbp larger than the average genome of sequenced *B. coagulans* strains, with expanded carbohydrate metabolism and mobilome. Functional genomics identified a well-equipped genetic portfolio for utilizing a wide range of C5 (xylose, arabinose), C6 (glucose, mannose, galactose), and C12 (cellobiose) sugars present in biomass hydrolysates, which was validated experimentally. For growth on individual xylose and glucose, the dominant sugars in biomass hydrolysates, B-768 exhibited distinct phenotypes and proteome profiles. Faster growth and glucose uptake rates resulted in lactate overflow metabolism, which makes *B. coagulans* a lactate overproducer; however, slower growth and xylose uptake diminished overflow metabolism due to the high energy demand for sugar assimilation. Carbohydrate Transport and Metabolism (COG-G), Translation (COG-J), and Energy Conversion and Production (COG-C) made up 60–65% of the measured proteomes but were allocated differently when growing on xylose and glucose. The trade-off in proteome reallocation, with high investment in COG-C over COG-G, explains the xylose growth phenotype with significant upregulation of xylose metabolism, pyruvate metabolism, and TCA cycle. Strain B-768 tolerates and effectively utilizes inhibitory biomass hydrolysates containing mixed sugars and exhibits hierarchical sugar utilization with glucose as the preferential substrate.

IMPORTANCE. The robustness of *B. coagulans* makes it a valuable microorganism for biotechnology applications, yet this phenotype is not well understood at the cellular level. Through phenotypic characterization and systems analysis, this study elucidates the functional genomics and robustness of a novel, undomesticated strain, *B. coagulans* B-768, capable of utilizing inhibitory switchgrass biomass hydrolysates. The genome of B-768, enriched with carbohydrate metabolism genes, demonstrates high regulatory capacity. The coordination of proteome reallocation in Carbohydrate Transport and Metabolism (COG-G), Translation (COG-J), and Energy Conversion and Production (COG-C) is critical for effective cell growth, sugar utilization, and lactate production via overflow metabolism. Overall, B-768 is a novel, robust, and promising *B. coagulans* strain that can be harnessed as a microbial biomanufacturing platform to produce chemicals and fuels from biomass hydrolysates.

Keywords: Bacillus coagulans, B-768, lactate overproducer, overflow metabolism, carbohydrate metabolism, robustness, biomass hydrolysates, switchgrass, thermophile, proteome reallocation.

52 **INTRODUCTION**

53 Lignocellulosic biomass derived from bioenergy crops (e.g., poplar, switchgrass) or
54 agricultural residues (e.g., corn stover) are renewable and sustainable feedstocks(1, 2). These
55 feedstocks can be produced at a scale of 1 billion tons per year in the US, reducing reliance on
56 petroleum to make fuels, chemicals, and materials(3). Lignocellulosic biomass is comprised of
57 cellulose, hemicellulose, and lignin(4). These polymers can be isolated to make consumables(5,
58 6), advanced materials(7), and other valuable commodities. Alternatively, these polymers can be
59 further broken down to monomers through chemical pretreatment followed by enzymatic
60 saccharification to generate biomass hydrolysates that consist of pentose (C5) and hexose (C6)
61 sugars and byproducts (e.g., organic acids, furans, and phenolics). Through fermentation,
62 microbial cell factories can be harnessed as biocatalysts to convert these sugars into various classes
63 of fuels, chemicals, and materials(2, 8, 9) including carboxylic acids(10), alcohols(11-13),
64 aldehydes(14), ketones(15), amines(16), esters(17, 18), polyhydroxyalkanoates(19), and protein-
65 based polymers(20). Biomanufacturing is thus important for a circular bioeconomy where
66 renewable and sustainable feedstocks can be effectively utilized to make renewable goods(21).

67 One technical barrier to biomanufacturing is creating robust microbial catalysts capable of
68 transforming biomass hydrolysates into fuels, chemicals, and materials. Robustness is defined as
69 the efficacy by which microbes can convert biomass hydrolysates into a target chemical under
70 harsh conditions that cause biocatalyst poisoning(22, 23). Robustness is a complex phenotype that
71 requires controlled expression of multiple genes. For instance, the effective assimilation of C5
72 and C6 sugars in biomass hydrolysates is a complex phenotype, requiring a highly regulated gene
73 network(24). Coping with chemical inhibitors such as pretreatment byproducts in biomass
74 hydrolysates and target products generated during fermentation forces cells to optimize their

75 cellular resources at the systems level(25). Therefore, deploying robust microbial catalysts,
76 whether natural isolates or engineered microorganisms, for efficient conversion of lignocellulosic
77 biomass to a target product is critical for biomanufacturing.

78 The robustness and unique metabolic capability of *Bacillus coagulans* make it a promising
79 biomanufacturing platform. *B. coagulans* (also known as *Weizmannia*/*Heyndrickxia coagulans*) is
80 a GRAS (generally recognized as safe) Gram-positive bacterium and facultative thermophilic
81 anaerobe. *B. coagulans* grows on a variety of carbohydrates(26-28) at a wide range of
82 temperatures(29) and pHs(30) and is capable of overproducing lactate(31), thermostable
83 enzymes(31), and antimicrobial peptides(31-33). Due to its unique metabolic capability and
84 inherent robustness, *B. coagulans* is also utilized for probiotic formulations(34). Even though it is
85 a promising biomanufacturing platform, the fundamental understanding of its robustness and
86 underlying genetics is limited.

87 In this study, we characterized the robustness physiology of *B. coagulans* B-768, a novel,
88 undomesticated strain. We first assessed its unique metabolic capability by growing it on various C5
89 (arabinose, xylose), C6 (glucose, galactose, mannose), and C12 (cellobiose) sugars at a wide range
90 of temperatures and evaluated its tolerance to high lactate concentrations. Genome sequencing and
91 annotation were performed to provide insights into its observed metabolic capability. Subsequent
92 characterization of B-768 growing on xylose, glucose, a mixture of xylose and glucose, and biomass
93 hydrolysate, coupled with quantitative proteomics, validated the functions of genes involved in sugar
94 utilization and elucidated how cells dynamically reallocate their proteomes in response to different
95 carbon sources. Finally, we examined the regulation of sugar utilization in B-768 and uncovered the
96 cellular processes and molecular drivers responsible for B-768's robust growth on undetoxified
97 hydrolysates.

98

99 # RESULTS AND DISCUSSION

100 ## *B. coagulans* B-768 is a robust biomanufacturing platform microorganism

101 Utilization of a wide range of biomass-derived sugars is crucial for a robust
102 biomanufacturing platform microorganism. Strain B-768 was grown on glucose, xylose, and
103 cellobiose -the dominant sugars present in biomass hydrolysates -at a range of temperatures (30–
104 59 °C, Figs. 1A–C). Optimum cell growth was observed between 45–53 °C with a maximum
105 growth rate of 0.4 h^{-1} on glucose and 0.2 h^{-1} on xylose or cellobiose. Next, B-768 was grown in
106 media containing galactose, mannose, or arabinose at 50 °C in addition to the previous sugars (Fig.
107 1D). Glucose and mannose were the most efficiently used carbon sources, followed by galactose,
108 xylose, arabinose, and cellobiose, which all yielded similar maximum specific growth rates and
109 maximum cell biomasses (Figs. 1D, S1A). In addition to the assimilation efficiencies of various
110 carbon sources, tolerance to high product concentrations is critical to determine cellular
111 robustness. Since *B. coagulans* is well-known for its high lactate production, we evaluated the
112 growth of B-768 in cultures containing various lactate concentrations with glucose as a sole carbon
113 source (Figs. 1E, S1B). The maximum specific growth rate was reduced as lactate concentration
114 was increased, and B-768 could tolerate up to at least 30 g/L lactate. Since this experiment was
115 performed in a pH-uncontrolled environment, it was hypothesized that higher lactate tolerance
116 could be achieved when the medium pH was maintained at an optimum level. To evaluate this
117 hypothesis, a pH-controlled fermentation was performed with 80 g/L glucose as the sole carbon
118 source. As expected, when the pH was maintained at 6.5, B-768 produced up to 60 g/L lactate at
119 92.7% of the theoretical maximum yield (Fig. 1F). These results highlight the robustness of B-768

120 for metabolizing biomass-derived sugars, growing over a broad range of temperatures, and
121 selectively producing lactic acid at high yields.
122
123 **Functional and comparative genomics of *B. coagulans* B-768**
124 ***Genome sequence of B-768 and its relatedness to other B. coagulans strains.*** The genome
125 of B-768 was sequenced in an attempt to elicit the genetic basis of its physiological robustness.
126 The genome assembly size of B-768 is 3,944,476 base pairs long with 45.7% GC content, which
127 is 630 Kbp larger than the average *B. coagulans* genome and is the largest reported genome for *B.*
128 *coagulans* (Fig. 2). Strain B-768 contains 4,059 genomic features, of which 3,863 (95.2%) are
129 coding sequences (CDS). Phylogenomic analysis of a 55-strain *B. coagulans* pan-genome
130 compared to model strains 36D1 and DSM1 showed that B-768 belongs to the same clade as 36D1
131 (clade A) and is radically diverged from DSM1 (clade B, Fig. 3A). Also, its genome is 11% larger
132 than 36D1 and 17% larger than DSM1 (Table 1). Concordantly, there are ~20% more CDS in B-
133 768 compared to 36D1 or DSM1. Strains B-768 and 36D1, but not DSM1, are capable of
134 metabolizing C5 sugars (e.g., xylose and arabinose)(31, 35-37). Other strains reported to
135 metabolize xylose, including NL01(27, 38) and DSM 2314(39), also belong to clade A. The ability
136 to efficiently use C5 sugars could aid strains in occupying an ecological niche and incentivize the
137 acquisition of relevant genomic material through vertical and horizontal gene transfers. This
138 hypothesis is supported by the fact that genomes from clade A are on average ~171 Kbp larger
139 than those for clade B. Though further characterization of xylose and arabinose usage in *B.*
140 *coagulans* strains is needed to confirm this hypothesis, C5 metabolism could partially explain the
141 genetic differences underlying the topology of the *B. coagulans* pan-genome.

142 ***The larger genome of B-768 provides potential gains-of-function for enhanced cellular***
143 ***robustness***. To better understand the biological functions that may be associated with the added
144 genomic material of B-768, we conducted a comparative COG (Clusters of Orthologous Genes)
145 analysis by calculating the percent change of CDS belonging to each COG category between B-
146 768 and its closest reference, 36D1 (Fig. 3B–E). The percent change was calculated as follows:
147 $100 * \frac{N_{B-768} - N_{36D1}}{N_{36D1}}$, where N is the number of proteins belonging to the specified COG. Several
148 putative phage proteins found using PHASTEST(40) not recognized by automated COG
149 annotation(41) were manually added to the Mobilome COG. The percent change of the top 10
150 COGs is shown in Fig. 3B. B-768 contains more genes than 36D1 for nearly every COG category
151 with several categories being heavily expanded, such as the Mobilome (COG-X), Intracellular
152 Trafficking, Secretion, and Vesicular Transport (COG-U), Carbohydrate transport and metabolism
153 (COG-G), and Transcription (COG-K, Fig. 3B). Detailed examination of the individual proteins
154 involved in these COGs can shed light into the robustness of B-768, specifically COG-G and COG-
155 K due to their relevance to carbon utilization (Fig. 3C & 3D) and COG-X due to its role in
156 horizontal gene transfer and genome composition (Fig. 3E).
157 ***Unique carbohydrate metabolism, transport, and regulation of B-768***. Carbohydrate
158 Metabolism and Transport is the largest functional category in B-768, underlying the observed
159 robust carbon metabolism. B-768 contains 52.4% more proteins in COG-G than 36D1, and more
160 proteins were identified for all protein classes (Fig. 3C). Top protein classes include arabinose
161 efflux permeases, Na+/melibiose symporters/transporters, sugar kinases, and sugar permeases.
162 The overrepresentation of transporters among this group suggests B-768's vigorous carbon
163 metabolism is partly due to improved uptake of carbon substrates. Transcriptional regulators are
164 known to play key roles in regulating the use of carbon sources. A breakdown of the COG-K

165 reveals B-768 has at least 16 more transcriptional regulators than 36D1, belonging to the
166 LacI/PurR, LysR, ArsR, and GntR families (Fig. 3D). LacI and PurR regulators are mostly
167 allosteric repressors of carbon and nucleotide synthesis, respectively, and may control one (e.g.
168 LacI) or many (e.g. PurR) operons(42). Given the ability of B-768 to utilize various carbon sources
169 (Fig. 1D), an enlarged complement of LacI/PurR regulators likely helps coordinate the use of
170 available sugars. LysR and GntR regulators act globally as either activators or repressors of various
171 cellular processes including, but not limited to, metabolism, virulence, motility, and intercellular
172 communication(43, 44). ArsR regulators repress operons linked to metal stress under normal
173 physiological conditions. Upon binding with multivalent metal or metalloid ions, the associated
174 operons are derepressed and can provide resistance to otherwise toxic concentrations of
175 metals/metalloids(45). An excess of 6 ArsR regulators in B-768 may enable it to survive in metal-
176 rich environments where other *B. coagulans* strains cannot thrive.

177 ***Mobilome of B-768 reveals its capability to expand its genome***. B-768 contains 168%
178 more proteins in its Mobilome—which includes prophages, transposons, and plasmid mobilization
179 and maintenance machinery—compared to 36D1 (Fig. 3E). Six more transposases, which are
180 capable of rearranging, adding, or removing genomic material, were identified from B-768's
181 chromosome. The most significant portion of B-768's expanded Mobilome, however, is attributed
182 to two putative prophage regions that encode 32 CDS. In contrast, 36D1 has no prophages or
183 phage-related proteins. Prophage-like entities are commonly found in probiotic strains and can
184 provide resistance to similar phages(46, 47). The first prophage region is 32.7 kb long (genomic
185 coordinates: 1024169–1056950) and is predicted to be incomplete due to the absence of various
186 necessary phage genes such as portal, capsid, terminase, and tail genes. It does, however, encode
187 for 2 integrases, 1 protease, 1 endonuclease, 1 antirepressor, and several other unannotated phage-

188 like proteins which may contribute to bacterial fitness and/or horizontal gene transfer. The second
189 prophage is 38.3 kb long (genomic coordinates: 1805785–1844080) and is putatively intact,
190 possessing all major proteins required for phage infection. Many of the closest homologs for B-
191 768's putative phage proteins are from *Bacillus* phages, but several come from *Corynebacterium*,
192 *Agrobacterium*, and *Enterococcus* phages as well, meaning the exact origin and classification of
193 the prophage regions remain unclear. The existence of prophages in *B. coagulans* strains has been
194 previously reported, but in all cases the phages were deemed non-functional(48, 49). Given the
195 well-established role of bacteriophages in horizontal gene transfer, the presence of two putative
196 prophages could help explain the origin of B-768's expanded genetic repertoire. An operational
197 phage in *B. coagulans* could potentially be useful for introducing DNA via transduction, enabling
198 various genetic engineering approaches. Together, these findings provide a glimpse into the
199 expanded genome of B-768 that facilitates its extraordinary cellular robustness.

200 ***Defense systems in B-768: restriction-modification and CRISPR-Cas.*** Bacteriophage
201 contamination is a common problem in bacterial fermentation and can lower product yields and
202 either slow or halt fermentnations(50). Bacteria have developed numerous defense systems for
203 rebuffing bacteriophage infection, including innate restriction-modification (R-M) and adaptive
204 CRISPR (clustered regularly interspaced short palindromic repeats)-Cas (CRISPR-associated). To
205 elucidate the robustness of B-768, we evaluated its innate and adaptive defense systems to assess
206 its potential resistance to phage infection and suitability for industrial application.

207 Restriction-modification systems recognize and cut foreign DNAs having different
208 methylation patterns than the host. R-M systems are categorized into four types, Type I–IV, based
209 on genetic structure and biochemical function. Type I systems are multi-subunit complexes
210 composed of the R (restriction endonuclease), M (methyltransferase), and S (DNA-specificity)

211 subunits expressed from a single operon. Type II and III systems are comprised of restriction
212 endonuclease and methyltransferase subunits, but while Type II R and M proteins function
213 independently, Type III restriction enzyme activity requires an R-M complex. Type IV systems
214 are effectors that may be encoded by either 1 or 2 genes(51). Type I, II, and III restriction
215 endonucleases recognize and cleave unmethylated DNA at a specific DNA motif, while Type IV
216 restriction endonucleases cleave DNA that is methylated differently from the host. Our genomic
217 analysis shows that B-768 has 11 predicted R-M proteins including 7 Type I, 2 Type II, and 2 Type
218 IV proteins (Table 2). No Type III R-M proteins were found. In B-768, a complete Type I R-M
219 system is encoded within a single operon spanning from 2754339–2761240. We found that B-768
220 also has 4 additional Type I R submodules co-localized from 3201231–3202333, but it is unclear
221 whether these isolated proteins participate in Type I R-M activity in B-768. Both Type II R-M
222 proteins in B-768 are contained in an operon from 2170437–2176691. B-768's Type IV genes are
223 co-localized, meaning they likely encode for a 2-subunit effector. In total, B-768 has 3 distinct and
224 intact R-M systems that enable robust restriction of foreign DNAs.

225 CRISPR-Cas systems are functionally distinct immune systems found in archaea, bacteria,
226 and even huge bacteriophages(52-54). These systems work in a two-step process: adaptation and
227 interference. In adaptation, stretches of foreign DNA (protospacers) are integrated into CRISPR
228 arrays within the host genome and stored for future use. These short fragments are called spacers.
229 During interference, spacers are transcribed, form a complex with Cas effector proteins, and guide
230 a ribonuclease to a cognate protospacer, where the target DNA is cleaved. Our genomic analysis
231 found that B-768 possesses 5 putative CRISPR arrays containing 145 spacers. Three CRISPR
232 arrays have no associated Cas proteins near them and 2 have accompanying Type I-B and I-C
233 CRISPR machinery (Fig. 3F). The Type I-B CRISPR system is predicted to have complete

234 interference and adaptation arsenals, while the Type I-C system appears to only possess
235 interference-related genes. Analysis of B-768's entire set of spacers reveals CRISPR RNAs
236 targeting both phages and plasmids, which indicates B-768 has a history of deploying CRISPR-
237 Cas against foreign invaders of various origins (Table 3). In addition to robust and programmable
238 defense against deleterious phages, B-768's endogenous CRISPR systems could hold promise for
239 editing *B. coagulans* and other industrially relevant thermophiles.

240 ***Lignocellulosic biomass-derived sugar metabolism in B-768.*** The C6 sugars (e.g.,
241 glucose) are mainly transported inside the cells using the phosphoenolpyruvate
242 (PEP):carbohydrate phosphotransferase system (PTS) (Dataset 1). The phosphorylated sugars
243 (e.g., glucose-6-phosphate) are assimilated via the Embden-Meyerhof-Parnas (EMP) and/or
244 Entner-Doudoroff (ED) pathways. We identified the full set of necessary genes for the EMP
245 pathway in B-768 (Fig. 4, Dataset 2). On the other hand, B-768 contains an incomplete ED
246 pathway due to the absence of 6-phosphogluconate dehydratase (EDD), which converts 6-P-
247 gluconate into 2-keto-3-deoxy-6-phosphogluconate (Fig. 4, Dataset 2). B-768 does, however,
248 possess 6-phosphogluconate dehydrogenase (6PGD) that converts 6-phosphogluconate into
249 ribulose-5-phosphate, one of the end products in the pentose phosphate pathway. In summary,
250 glycolysis is the primary pathway for C6 sugar degradation in B-768, with possible metabolic flux
251 through a hybrid ED and pentose phosphate pathway route.

252 Since B-768 grows on xylose (Figs. 1B, 1D), it is expected that B-768 contains xylose
253 assimilation genes. Transport is the first step of carbon utilization and B-768 contains two putative
254 xylose transporters, xylose H+-symporter (XYLT, encoded by *xylT*) and an ABC-type xylose
255 transporter (*xylFGH*). These were identified using 36D1 xylose transporters as reference genes
256 (Dataset 1). Xylose transported inside of the cell via xylose transporters is metabolized by two key

257 enzymes: xylose isomerase (XI, encoded by *xylA*), which converts D-xylose into D-xylulose, and
258 xylulokinase (XK, encoded by *xylB*), which converts D-xylulose into D-xylulose-5-phosphate.
259 Typically, *xylA*, *xylB*, and *xylT* are encoded alongside *xylR*—a transcriptional repressor of the *xyl*
260 operon(55, 56)— in a single operon, but in B-768 *xylT* is located separately over 1 Mbp away (Fig.
261 4, Dataset 2). Once xylose is converted into D-xylulose-5-phosphate, it can be further assimilated
262 by either the pentose phosphate pathway (PPP) or the phosphoketolase pathway (PKP). The PKP
263 results in equimolar production of lactate and acetate in lactic acid bacteria(57), while the PPP
264 yields homolactic acid, making the PPP desirable for lactate production from pentoses(36). B-768
265 contains a full complement of PPP genes but lacks the critical PKP enzyme, phosphoketolase
266 (Dataset 2). Given the lack of phosphoketolase, B-768 mainly utilizes the homolactic acid PPP to
267 degrade xylose, setting it apart from most other lactic acid bacteria that prefer the PKP(58). This
268 is an essential trait for ensuring high lactic acid yields on cellulosic sugar mixtures.

269 B-768 also contains genes that putatively allow it to use xylosides. Xylosides are released
270 when xylan or xyloglucan are depolymerized and may be converted into D-xylose by α- or β-
271 xylosidases(59). Putative xyloside symporter (*xynT*) and α-xylosidase (*xylS*) genes were found in
272 the *xyl* operon in B-768, and three β-xylosidases were scattered throughout the rest of the genome.
273 While closely related strain 36D1 has a copy of *xynT*, it does not possess any known
274 xylosidases(31). To determine the origin of the four xylosidase proteins, BLASTp analysis was
275 performed against the non-redundant protein database (Table 4). This search revealed homologs
276 in closely related species for all but one of the xylosidases. Enzyme 4-beta-xylosidase located from
277 665440–666999 had top hits primarily belonging to *Enterococcus* spp., with the top hit occurring
278 in *Melissococcus plutonius*. This provides another example of *B. coagulans* B-768 utilizing

279 horizontal gene transfer to expand its carbon-utilizing potential. This is useful trait because xylan
280 oligomers are competitive inhibitors of cellulases.

281 Cellobiose assimilation is key to bypassing carbon catabolite repression (CCR), wherein
282 xylose assimilation is inhibited by glucose. Cellobiose utilization in *B. coagulans* is mainly
283 mediated by the five-member CELO1 operon encoding three phosphotransferase system (PTS)
284 subunits EIIA (*celA*), EIIB (*celB*), EIIC (*celC),* a 6-phospho-β-glucosidase (*pbgl*), and a
285 transcriptional regulator (*celR*)(27). Some strains like *B. coagulans* NL01, 36D1, 2-6, and HM08
286 have an additional cellobiose operon, CELO2, which encodes paralogs of *celABCR* along with an
287 unknown protein (*celX*)(27). Using 36D1 as a reference strain, we identified cellobiose
288 assimilation pathway genes in B-768. In B-768, both CELO1 and CELO2 are fully intact and
289 located from 1361260–1367923 and 1464816–1469898, respectively. Notably, B-768 contains
290 two additional copies of 6-phospho-β-glucosidase—the enzyme catalyzing the rate-limiting step
291 in the breakdown of cellobiose to glucose(60, 61)—which may improve cellobiose catabolism.

292 Due to B-768's metabolic capability to assimilate galactose, mannose, and arabinose (Fig.
293 1D), we also investigated the catabolic pathways of these monomeric sugars. Galactose
294 metabolism in bacteria is mediated by the ubiquitous four-enzyme Leloir pathway, containing the
295 enzymes galactose mutarotase, galactokinase, galactose-1-phosphate uridylyltransferase, and
296 UDP-galactose 4-epimerase(62). B-768 possesses all four genes in an operon from 1161267–
297 1165598 with an additional copy of galactose mutarotase (Dataset 1). Mannose metabolism in
298 *Bacillus subtilis* is mediated by a mannose transporter (*manP*), a mannose-6-phosphate isomerase
299 (*manA*), and a mannose activator (*manR*)(63). In *B. coagulans*, mannose metabolism is much the
300 same, except the mannose transporter is mediated by the mannose PTS system encoded by 4
301 subunit genes (*manEIIABCD)* instead of a single gene (Dataset 1). B-768 possesses homologs for

302 these genes, but *manA* is absent from the operon containing *manR* and *manEIIABCD* (Dataset 1).
303 All canonical arabinose utilization proteins are present in B-768, many of which possess several
304 putative paralogs (Dataset 1). Most of these paralogs are either for arabinose/arabinan permeases
305 or transcriptional regulators of the *ara* regulon. This is consistent with the finding that most of B-
306 768's genes involved in carbon metabolism putatively encode for C5/C6 sugar kinases, permeases,
307 and transcriptional regulators (Fig. 3C). Overall, B-768 has accrued an extensive array of genes
308 dedicated to metabolizing a wide variety of sugars.
309

310 **Distinct phenotypes and proteomes of B-768 for utilization of biomass-derived sugars**

311 ***B-768 grew faster on glucose than xylose, resulting in lactate overflow metabolism.*** Since
312 xylose and glucose are the most dominant C5 and C6 sugars in biomass hydrolysates, we first
313 aimed to elucidate the phenotypes and metabolic responses of B-768 growing on these sugars.
314 When supplied with 10 g/L glucose, B-768 grew at a rate of 0.59 ± 0.01 h^{-1}. Within 8 h, it achieved
315 a maximum growth of 3.45 ± 0.11 OD_{600} and exhausted all the glucose with a glucose uptake rate
316 of 1.67 ± 0.15 g glucose/OD_{600}/h (Fig. 5A, 5B). B-768 produced lactate as the major fermentative
317 product at a titer of 8.72 ± 0.05 g lactate/L, a productivity of 1.46 ± 0.03 g lactate/OD_{600}/h, and a
318 yield of 0.89 ± 0.01 g lactate/g glucose (~90% of the maximum theoretical yield). In contrast,
319 when growing on xylose, B-768 exhibited a much slower growth rate of 0.32 ± 0.01 h^{-1}. After ~24
320 h, cells reached the growth of 3.45 ± 0.10 OD_{600} and only consumed 3.52 ± 0.45 g/L out of ~10
321 g/L xylose available with a xylose uptake rate of 0.35 ± 0.04 g xylose/OD_{600}/h (Fig. 5A, 5B). B-
322 768 only produced lactate at a titer of 1.57 ± 0.12 g lactate/L, a productivity of 0.07 ± 0.01 g
323 lactate/OD_{600}/h, and a yield of 0.18 ± 0.02 g lactate/g xylose. Overall, faster growth and glucose
324 uptake rate made B-768 reroute high carbon flux toward lactate biosynthesis. Even though B-768

325 reached the same cell biomass for growth on xylose after 24 h, slower growth and xylose uptake
326 rate shifted its carbon flux mainly towards biomass synthesis at the expense of lactate production.
327 ***B-768 exhibited distinct proteomes for growth on glucose and xylose.*** To elucidate the
328 phenotypic differences for B-768 grown on glucose and xylose at the cellular level, cultures were
329 sampled at mid-exponential phase for quantitative proteomics. Principal component analysis of
330 glucose and xylose samples revealed highly distinct proteomes (Fig. 5C). Differential expression
331 analysis was then performed on the glucose- and xylose-only samples and the number of
332 significantly altered proteins was tallied for each COG category (Fig. 5D). The results showed that
333 proteomes had shifted across the COG categories to varying degrees. Most significantly perturbed
334 proteins in cells growing on xylose compared to on glucose belong to the Carbohydrate Transport
335 and Metabolism (COG-G) and Energy Production and Conversion (COG-C) categories. As
336 expected, both the major xylose utilization proteins—xylose isomerase and xylulokinase—were
337 among the most xylose-upregulated proteins by 5.99 $\log_2$-fold (q-value = 4.17E-14) and 7.28 $\log_2$-
338 fold (q-value = 4.17E-14), respectively in the COG-G category (Fig. 4, Dataset 3). Among the PPP
339 proteins, ribose-5-phosphate isomerase (RPI) was significantly upregulated by 1.29 $\log_2$-fold (q-
340 value = 0.0478), while the rest were not significantly perturbed (Fig. 4, Dataset 3). Most of the
341 xylose downregulated proteins in COG-G were proteins involved in the EMP pathway, such as
342 triose phosphate isomerase (TPI), glyceraldehyde-3-phosphate dehydrogenase (GAPDH), enolase
343 (ENO), and pyruvate kinase (PK) by -1.9 $\log_2$-fold (q-value = 8.45E-3), -1.29 $\log_2$-fold (q-value
344 =3.53E-3), -1.36 $\log_2$-fold (q-value = 0.012), and -1.48 $\log_2$-fold (q-value = 2.93E-4), respectively
345 (Fig. 4, Dataset 3). Lactate dehydrogenase (LDH) is also significantly downregulated in xylose
346 relative to glucose by -2.63 $\log_2$-fold (q-value = 1.83E-4) at the measured timepoint (Fig. 4, Dataset
347 3), which is consistent with the observed low lactate production (Fig. 5B). In COG-C, several

348 enzymes involved in pyruvate metabolism, such as formate C-acetyltransferase (or pyruvate
349 formate lyase, PFL), dihydrolipoamide dehydrogenase (DLD), and pyruvate dehydrogenase
350 subunits E1α and E1β (PDH) for converting pyruvate to acetyl-CoA, were significantly
351 upregulated in xylose by 5.71 $\log_2$-fold (q-value = 4.17E-14), 3.71 $\log_2$-fold (q-value = 4.17E-14),
352 3.44 $\log_2$-fold (q-value = 2.52E-6), and 3.1 $\log_2$-fold (q-value = 1.37E-13), respectively (Dataset
353 3). Enzymes that convert acetyl-CoA into acetate and ethanol were upregulated in xylose,
354 including acetyl-CoA synthetase (ACS), aldehyde dehydrogenase (ALDH), and alcohol
355 dehydrogenase (ADH), by 3.7 $\log_2$-fold (q-value = 1.24E-4), 4.86 $\log_2$-fold (q-value = 4.17E-14),
356 and 3.6 $\log_2$-fold (q-value = 1.03E-7), respectively (Dataset 3 and Fig. S4). Acetyl-CoA is also
357 passed into the TCA cycle, which is highly upregulated on xylose (Dataset 3 and Fig. S5).

358 ***Tradeoffs of proteome reallocation between carbohydrate metabolism and energy***
359 ***generation contributed to the differential growth on glucose and xylose***. We then investigated
360 how B-768 re-allocated its resources in response to glucose or xylose by summing the mass
361 fractions of all expressed proteins for each COG (Fig. 5E). The top 7 COGs, including COG-G, J
362 (Translation), C, E (Amino Acid Transport and Metabolism), F (Nucleotide Transport and
363 Metabolism), O (Posttranslation Modification, Protein Turnover, Chaperons), K, V (Defense
364 Mechanisms), M (Cell Wall/Membrane/Envelope Biogenesis), and H (Coenzyme Transport and
365 Metabolism), contributed up to 80% of the total measured proteomes as shown in Fig. 5E. The top
366 3 COGs, including G, J, and C, shared up to 60–65% of each measured proteome with a high
367 degree of variability for growth on glucose and xylose. Despite most significantly differential
368 proteins in COG-G being upregulated in xylose relative to glucose (Fig. 5D), the proteome mass
369 fraction allocated to COG-G was much higher when B-768 was grown on glucose compared to
370 xylose (29% Glu vs. 19% Xyl, Fig. 5E). This result indicates that protein expression was higher

371 even with fewer proteins in cells grown in glucose compared to cells grown in xylose. Consistent
372 with this hypothesis, B-768 also devoted significantly more resources to COG-J when grown on
373 glucose compared to xylose (22% Glu vs. 17% Xyl). Xylose-grown cells disproportionately
374 invested their resources in COG-C, presumably to offset the higher energy cost of transporting and
375 assimilating xylose (29% Xyl vs. 10% Glu, Fig. 5E).

376 To better elucidate how proteome reallocation is linked to the distinct phenotypes for B-
377 768 growing on glucose and xylose, the allocation of proteomes in COG-G and COG-C was
378 analyzed at a more granular resolution based on the relevant pathways (Fig. 5F–K). Enriched
379 pathways in the cells grown on xylose include the TCA cycle (6.78-fold, p-value < 0.0001, Fig.
380 5F), pyruvate metabolism (2.32-fold, p-value < 0.0001, Fig. 5G), and xylose metabolism (4.52-
381 fold, p-value = 0.0001, Fig. 5H), reiterating the trends observed from differential expression
382 analyses. Glucose-grown cells had slightly more investments into glycolysis (0.095-fold, p-value
383 < 0.0001, Fig. 5I), the pentose phosphate pathway (0.24-fold, p-value = 0.0063, Fig. 5J), and the
384 phosphotransferase system (0.18-fold, p-value = 0.0054, Fig. 5K). Overall, these findings reveal
385 that B-768 redistributed its proteome to accommodate the increased energy demand of
386 metabolizing xylose. To do this, various carbohydrate metabolism and energy production genes
387 were overexpressed, which direct carbon flux from xylose through the PPP to yield pyruvate.
388 Pyruvate is then converted into energy by channeling carbon and electron fluxes through pyruvate
389 metabolism, then the TCA cycle, followed by the electron transport system for ATP synthesis.
390 Although ATP synthase was not significantly different between xylose and glucose conditions,
391 other key proteins in the electron transport system were upregulated in xylose, such as NADH
392 dehydrogenase by 8.93 $\log_2$-fold (q-value = 3.63E-9) and succinate dehydrogenase by 3.72 $\log_2$-
393 fold (q-value = 2.42E-5). A significant reduction in LDH expression and lactate production, and

394 an increase in pyruvate metabolism correlates with the decreased lactate metabolism for growth
395 on xylose.

396 Lastly, amino acid reallocation in the measured proteomes was performed as previously
397 described to investigate the metabolic cost associated with switching to a xylose-utilizing
398 proteome(64) (Fig. 5L). Higher amounts of costly amino acids like tryptophan, tyrosine, and
399 phenylalanine are used in xylose-only conditions compared to glucose-only conditions(65).
400 Consistent with this finding, the 10 most highly expressed proteins in xylose possess 107% more
401 tryptophan, 37% more tyrosine, and 21% more phenylalanine than the top 10 proteins for glucose.
402 The greater demand for these costly amino acids could help explain the marked investment into
403 energy generation processes when B-768 is grown on. This finding suggests that supplementation
404 of *B. coagulans* B-768 with metabolically expensive amino acid(s) may alleviate part of the
405 metabolic burden due to amino acid biosynthesis and improve growth on xylose.

406

407 **Carbon catabolite repression is dominant in B-768 growing on glucose-xylose mixture and**
408 **switchgrass biomass hydrolysate**

409 As cellulosic hydrolysates contain a mixture of C5 and C6 sugars, it is important to
410 understand how B-768 regulates its metabolism for growth on mixed sugars. Carbon catabolite
411 repression (CCR) is a common regulatory mechanism used by bacteria to inhibit metabolism of
412 sub-optimal carbon sources (e.g., xylose) in the presence of a preferred substrate (e.g., glucose).
413 The diauxic growth observed when B-768 is grown on either a mixture of refined glucose and
414 xylose (G+X) or switchgrass hydrolysate (SGH), is evidence for a strong CCR on xylose
415 assimilation by glucose (Figs. 6A, 6B). Consistent with this observation (Fig. 6B), expression of
416 the *xyl* operon was heavily repressed (Figs. 6D, 6F). The effects of the observed mechanism can

417 be captured at the cellular level. Principal component analysis shows that all proteomes of cultures
418 growing in the presence of glucose were clustered tightly together, while those grown on xylose
419 were highly diverged (Fig. 6C).

420 To characterize CCR in *B. coagulans* B-768 and to select genetic targets for eliminating it,
421 canonical CCR proteins were quantified across a variety of growth conditions based on the CCR
422 model of the well-studied *B. subtilis* (Figs. 6D, 6E). To enable CCR, the master regulator CcpA
423 and its primary corepressor, histidine-containing phosphocarrier protein (HPr), or the secondary
424 catabolite corepressor (Crh), bind to catabolite-responsive elements (*cre*) located in the open
425 reading frame or promoter region of the target genes and block transcription(66) (Fig. 6D). Hpr
426 and Crh bind CcpA when phosphorylated at the Ser46 residue by the bifunctional HPr
427 kinase/phosphorylase (HPrK/P), whose activity is increased by the glycolytic intermediate,
428 fructose-1,6-bisphosphate (FBP)(67-69). CCR is further modulated by glucose-6-phosphate (G6P)
429 and FBP, which improve the DNA binding affinity of CcpA-(Hpr-Ser46-P), but not CcpA-(Crh-
430 Ser46-P)(70, 71). The results show that protein levels of CcpA, HPr, and HprK/P did not
431 significantly change between glucose-available and xylose-only conditions, agreeing with a
432 previous report (Fig. 6E)(72). While not statistically significant, phosphofructokinase-1 (PfkA),
433 which converts fructose-6-phosphate into FBP, is downregulated by 1.47 $\log_2$-fold changes in
434 xylose cultures relative to glucose. For growth on xylose, the FBP node of the EMP pathway can
435 be effectively bypassed because carbon passed through the PPP connects to glycolysis downstream
436 of FBP at glyceraldehyde-3-P. Lower concentrations of FBP would in turn downregulate the
437 kinase activity of HprK and DNA binding affinity of the CcpA effector complex (Fig. 6D).
438 Therefore, in B-768 relief of CCR on xylose appears to be likely due to reduced intracellular levels
439 of FBP.

440

441 **Growth hardiness of *B. coagulans* B-768 on complex biomass hydrolysate is explained by**
442 **proteomics**

443 A major challenge to utilizing lignocellulosic sugars is overcoming microbially inhibitory
444 chemicals formed during pretreatment and hydrolysis of the biomass. Depending on their
445 concentration, they can lead to extended lag phases, reduced product yields, or stalled
446 fermentations. While there are methods to mitigate these inhibitors, their drawbacks included
447 added cost, sugar loss, and reduced overall conversion efficiency(73, 74). Therefore, using
448 microbial biocatalysts that are robust to the presence of inhibitory compounds is paramount(75).
449 To elucidate the cellular robustness of B-768, its growth and lactate production were compared for
450 undetoxified dilute-acid switchgrass hydrolysate and a refined sugar control (Figs. 6A, 6B).
451 Surprisingly, no inhibitory effect on growth and lactate production was detected for B-768 grown
452 on SGH compared to refined sugars. This result indicates that B-768 can utilize glucose and—to
453 a much lesser extent—xylose present in undetoxified biomass hydrolysate without a reduction in
454 growth or lactate production, which makes this strain particularly attractive as a microbial
455 biomanufacturing platform.

456 To investigate the molecular drivers for the observed cellular robustness, comparative
457 proteomics was performed between cells grown in SGH and X+G (Fig. 6G). COG analysis was
458 performed on the 161 significantly differential proteins and all but 24 were assigned to a COG
459 category (Fig. 6H). Most proteins that could not be assigned a COG were annotated as hypothetical
460 proteins, but a few notable proteins included a putative transpose, a putative type VII secretion
461 system protein, a flagellar protein, and two sporulation proteins. All these proteins are stress-
462 implicated and probably play a role in helping B-768 adapt to hydrolysate toxicity. The top 3 COG

463 categories were COG-G (n = 24), COG-E (n = 14), and COG-T (n = 12). In terms of carbon
464 metabolism, all 3 major arabinose utilization proteins, L-arabinose isomerase, L-ribulokinase, and
465 L-ribulose-5-P 4-epimerase were significantly upregulated in SGH relative to X+G by 5.33 $\log_2$-
466 fold (q-value = 2.15E-14), 6.82 $\log_2$-fold (q-value = 5.98E-4), and 7.47 $\log_2$-fold (q-value =6.88E-
467 5), respectively. Additionally, 6-phospho-β-glucosidase (cellobiose utilization) and galactokinase
468 (galactose utilization) were upregulated in SGH by 9.06 $\log_2$-fold (q-value = 2.15E-14) and 4.07
469 $\log_2$-fold (q-value = 1.17E-4), respectively (Dataset 4). This result indicates that B-768 actively
470 metabolizes arabinose, cellobiose, and galactose when grown on unrefined biomass hydrolysates.
471 In addition to these proteins, several transporters of both the ABC and PTS varieties (n =
472 9), and chemotaxis-implicated proteins (n = 4) were significantly altered (Table 5). Similar
473 proteins were previously found to be significantly perturbed in *Clostridium acetobutylicum* in
474 response to phenolic inhibitors—common toxins found in biomass hydrolysates(76, 77). Another
475 inhibitor found in biomass hydrolysate is methylglyoxal(78, 79); therefore, it is noteworthy that
476 the most upregulated protein in SGH relative to X+G was glyoxylase II, a crucial enzyme for
477 detoxifying methylglyoxal(80). Finally, 10 putative transcriptional regulators were differentially
478 expressed (8 up, 2 down) with actuate transcriptional changes to accommodate growth in
479 hydrolysates (Table 5). Together, these results provide promising engineering targets for further
480 improving B-768's exceptional hydrolysate tolerance and demonstrate that B-768 displays a robust
481 and diverse proteomic response to hydrolysate toxicity, enabling favorable growth kinetics and
482 lactate titers in comparison to other industrial biocatalysts.
483

484 **CONCLUSIONS**

485 Through detailed phenotype characterization, comparative functional genomics, and
486 quantitative proteomic analyses, this study elucidates the mechanisms underlining the robustness
487 of undomesticated *B. coagulans* strain B-768,. Highlighted is the metabolic capability of B-768 to
488 utilize a wide range of C5 and C6 sugars at various temperatures, with glucose as the preferential
489 substrate. We created a high-quality genome assembly and annotation of *B. coagulans* B-768.
490 Essential to the robustness of B-768 is its larger genome including the expanded Carbohydrate
491 Transport and Metabolism and Mobilome, which enables improved sugar utilization and
492 horizontal gene transfer. A large set of genes devoted to its innate and adaptive defense
493 mechanisms should help *B. coagulans* resist phage attacks, which are a risk for bacterial industrial
494 fermentation processes. B-768 exhibits distinct proteomes for growth on glucose and xylose,
495 consistent with its observed phenotypes. Faster growth and glucose uptake rate resulted in lactate
496 overflow metabolism while slower growth and xylose uptake rate diminished lactate production.
497 This difference could be explained by the tradeoff in proteome reallocation between the
498 Carbohydrate Transport and Metabolism process and the Energy Generation and Production
499 process. B-768 can utilize biomass hydrolysates with various C5 and C6 sugars controlled by a
500 tightly regulated gene network. Overall, B-768 is a robust microbial biomanufacturing platform
501 that has potential beyond lactate fermentation. A fundamental understanding of its robustness
502 revealed in this study will be critical for rechanneling and tuning its metabolism for optimized
503 conversion of lignocellulosic biomass to chemicals, fuels, and materials beyond lactate.

504

505 **MATERIALS AND METHODS**

506 **Cell Culture**

507 ***Strains:*** *B. coagulans* strain B-768 (ATCC 10545=NRS-784) was obtained from the
508 NRRL Agriculture Research Service strain collection of the United States Department of
509 Agriculture (USDA) located in Peoria, IL. The strain was stored as glycerol stocks at -80 °C.
510
511 ***Media:*** The basal medium contained 1.5 g/L yeast extract, 100 mM sodium MES buffer
512 (pH 6.5), and mineral solution. The mineral solution contained: 2 g/L $(NH_4)_2SO_4$, 2 g/L KH_2PO_4,
513 2 g/L NaCl, 0.2 g/L $MgSO_4 \cdot 7H_2O$, 5 mg/L $MnSO_4 \cdot H_2O$, and 10 mg/L $FeSO_4 \cdot 7H_2O$. The
514 phosphate buffered saline (PBS) contained per liter: 8 g NaCl, 0.2 g KCl, and 1.44 g Na_2HPO_4,
515 adjusted to pH 7. 4 with NaOH.
516 The switchgrass hydrolysate (SGH) medium contained per liter: 10% (v/v) of concentrated
517 dilute acid pretreated SGH and 100 mM MES buffer (pH 6.5). The concentrated SGH solution was
518 prepared as previously described(81), which contained: ~70 g/L glucose and ~44 g/L xylose as the
519 main C5/C6 sugars of biomass hydrolysates. SGH was used at 10%w/w for bottle cultures.
520
521 ***High-throughput Microplate Growth Kinetic Experiments:*** Growth of B-768 on various
522 carbon sources (glucose, xylose, cellobiose, galactose, mannose, or arabinose) at various
523 temperatures (37, 40, 45, 47, 53, or 55 °C) was measured high-throughput using Bioscreen Pro™
524 (Oy Growth Curves Ab Ltd., Finland). B-768 was inoculated in basal medium containing no sugar
525 and grown at 50 °C overnight. Next day, overnight grown cells were diluted in fresh medium with
526 initial OD_{600} of 0.1 in total 300 µL and growth was monitored at 580 nm for 24 or 48 hrs. For the
527 lactate tolerance experiment, cells were prepared in a basal medium with 8 g/L glucose, and growth
528 was monitored at 50 °C using the Bioscreen Pro™.
529

530 ***Bottle Cultures:*** Seed cultures and media were prepared as described for the high-
531 throughput studies. Fermentations were conducted in 25 mL Pyrex bottles (Corning Life Sciences,
532 NY) filled with 20 mL of medium and incubated and mixed at 50 °C and 100 rpm, respectively.
533 Cultures were sampled for sugars (glucose and xylose), lactate, and OD_{600} using a 1 mL sample.
534 Proteomic samples (1 mL) were withdrawn, centrifuged, washed with chilled dH_2O, and the pellet
535 was stored at -80 °C.
536
537 ***pH-controlled Fermentations:*** Fermentations were maintained at pH 6.5 and 50 °C (unless
538 stated otherwise) and stirred at 300 rpm. Cells were inoculated to an initial OD_{600} of 0.1. The pH
539 was maintained by adding 4 N KOH. Cultures were sampled for OD_{600}, sugars, and fermentation
540 products.
541
542 **Analytical Methods**
543 ***High-Performance Liquid Chromatography (HPLC):*** Metabolites such as sugars and
544 acids (e.g. lactate and acetate) were measured by Bio-Rad HPX-87H column at 65 °C with 5 mM
545 sulfuric acid as a mobile phase using a Thermo high-performance liquid chromatography (Ultimate
546 3000) system equipped with a refractive index (RI).
547 ***Liquid Chromatography with Tandem Mass Spectrometry (LC-MS/MS):*** *B. coagulans*
548 strain B-768 cultured in the presence of various sugars (n = 3 per glucose, xylose, a mixture of
549 glucose and xylose, and switchgrass hydrolysate) were collected by centrifugation and cell pellets
550 prepared for LC-MS/MS based proteomics as previously described(82). All raw mass spectra for
551 quantification of proteins used in this study have been deposited in the MassIVE and
552 ProteomeXchange data repositories under accession numbers MSV000095240 (MassIVE) and

553 PXD053622 (ProteomeXchange), with data files available at
554 ftp://massive.ucsd.edu/v08/MSV000095240/.
555 ***Genome Sequencing:*** Genomic DNA of *B. coagulans* B-768 was subjected to Pacific Biosciences
556 (PacBio) long-read sequencing by DOE Joint Genome Institute (JGI)(83). A >10 kb Pacbio
557 SMRTbell® library was constructed and sequenced on the PacBio Sequel platform, which
558 generated 78,854 high-fidelity CCS reads totaling 696,902,661 bp. Reads >5kb were assembled
559 with Flye v2.8.3 using default settings(84, 85). The final draft assembly contained 1 contig in 1
560 scaffold, totaling 3,944,476 bp in size, and was 99.95% complete according to CheckM(86). The
561 input read coverage was 181.4x. The final draft assembly was annotated using the Integrated
562 Microbial Genomes Annotation Pipeline (IMGAP) v5.1.1. The whole-genome assemblies and
563 annotation were deposited at DDBJ/EMBL/GenBank (Bioproject ID: PRJNA1123721).
564
565 **Bioinformatics and Data Analysis**
566 ***CRISPR System and Spacer Identification:*** CRISPR system prediction was performed
567 using CRISPRCasTyper v1.8.0 with default settings(87). For identification of spacer hits on
568 plasmids, nucleotide sequences for the entire NCBI collection of bacterial plasmid sequences were
569 downloaded from PLSDB v. 2021_06_23_v2(88) and used to construct a BLASTn database
570 against which the JGI-predicted CRISPR spacers were blasted using the blastn-short algorithm
571 with default settings. Hits with e-value < 0.05 were retained and the top hit for each spacer was
572 chosen as the target source. For identification of spacer hits on phages, SpacePHARER
573 v5.c2e680a(89) was used with the GenBank_phage_2018_09 database and default settings.
574 ***Restriction-Modification Annotation:*** All B-768 protein sequences were searched against
575 the complete REBASE database using BLASTp v2.15.0+ with default settings. Hits were filtered

576 down to those with a percent identity >60% and alignment coverage >80% (alignment length/query
577 length). Hits were then sorted by ascending e-value and the top hit for each query was retained. 11
578 hits remained and all had e-values < 7.5E-42. These were considered bonafide R-M homologs and
579 the REBASE classification was used to assign the type.

580 ***Circular Genome Map:*** Proksee v5.2.1(90) was used to generate a circular genome map
581 for *B. coagulans* B-768 from functional annotation provided by JGI. GC content and skew were
582 calculated using the built-in function in Proksee. COG mapping was performed manually using
583 the feature upload tool and the output from COGclassifier v1.0.5(91). Prophage regions were
584 predicted using PHASTEST v3.0 and mapped using the feature upload tool(40).

585 ***Pan-genome Phylogeny:*** Genome sequences of all RefSeq *B. coagulans* strains, except
586 RUG1433, were downloaded from NCBI. A core-genome alignment was performed on the pan-
587 genome using Parsnp v1.7.4 with default settings(92). A recombination-aware maximum
588 likelihood tree was then constructed from the core-genome alignment using Gubbins v3.2.1 with
589 default settings(93).

590 ***Proteomics:*** The resulting MS/MS spectra acquired from the Q Exactive MS were searched
591 against the *B. coagulans* B-768 proteome database appended with common protein contaminants
592 using the SEQUEST HT algorithm in Proteome Discoverer v.2.5 (Thermo Scientific) and peptide
593 spectrum matches (PSMs) scored and filtered with Percolator (settings and dynamic/static mods
594 described in Walker *et al*'s study(82)). Peptides (FDR < 1%) were then quantified by
595 chromatographic peak area and derived abundances mapped back to each peptide's respective
596 protein and peptide abundance summed to estimate protein-level abundances. Protein abundances
597 were then $\log_2$ transformed, normalized by LOESS, and median centered using InfernoRDN(94).
598 Missing values were imputed, and statistical tests (T-test and ANOVA) performed using Perseus

599 v2.0.7.0(95). Log_2 transformed and imputed protein abundance data were analyzed using the DEP
600 R package v1.24.0(96). Significant proteins were filtered out based on a 5% FDR and minimum
601 log_2 fold-change of 1.

602 ***Proteome Reallocation:*** Based on the mass fractions of each protein per sample, proteome
603 reallocation was calculated by dividing each raw protein abundance by the sum of all protein
604 abundances for a given sample and summed up across the indicated categories of interest(64, 82).
605 COG annotations were mapped onto predicted protein sequences from JGI using COGclassifier
606 v1.0.5(91). All calculations were performed in R v4.3.0.

607 ***Amino Acid Allocation:*** Analyses of amino acid allocation in the measured proteomes
608 were determined based on the formulation previously described(64, 82). All the calculations were
609 performed in Python v3.8.16 and the outputs were analyzed in R v4.3.0.

610 ***Kinetics:*** The specific growth rate was determined by assuming that cell growth follows
611 the first-order kinetics (Equation 1).

612 $$\frac{dX}{dt} = \mu \cdot X \quad (1)$$

613 where X (g DCW/L) is cell mass, t (h) is the culturing time, and μ (1/h) is the specific growth rate.
614 Note that DCW represents dry cell weight and is linearly correlated with the measured cell optical
615 density (OD_{600}). The substrate uptake rate was determined as follows (Equation 2):

616 $$-r_S = \mu \cdot Y_{S/X} \quad (2)$$

617 where r_S (g/g DCW/h) is the specific substrate uptake rate and $Y_{S/X}$ (g substrate/g CDW) is the
618 yield of a substrate (e.g., glucose) to cell mass. The product formation rate was determined as
619 follows (Equation 3):

620 $$r_P = \mu \cdot Y_{P/X} \quad (3)$$

621 where r_P (g/g DCW/h) is the specific substrate uptake rate and $Y_{P/X}$ (g substrate/g CDW) is the
622 yield of a product (e.g., lactate) to cell mass.

623 ***Calculation of Optimal Growth Temperatures:*** Optimal growth temperatures on various
624 sugars were determined by fitting maximum growth rate versus temperature with a non-linear
625 model (Continuous hinge function. Segmental regression lines with gentle connection, least
626 squares fit) using GraphPad Prism v10.2.3.

627

628 **ACKNOWLEDGEMENTS**

629 This research was funded by the DOE BER award (DE-SC0022226 to CTT, RJG, BD).
630 The sequencing project was supported by the Center for Bioenergy Innovation (CBI), U.S.
631 Department of Energy Bioenergy Research Centers, funded by the Office of Biological and
632 Environmental Research in the DOE Office of Science. The work (Project IDs # 510751, 509417)
633 conducted by the U.S. Department of Energy Joint Genome Institute, a DOE Office of Science
634 User Facility, is supported under Contract No. DE-AC02-05CH11231. Dien, Jackson, and
635 Slininger received financial support from the U.S. Department of Agriculture, Agricultural
636 Research Service, United States (CRIS Numbers 5010-41000-189). The mention of trade names
637 or commercial products in this article is solely for the purpose of providing scientific information
638 and does not imply recommendation or endorsement by the U.S. Department of Agriculture.
639 USDA is an equal opportunity provider and employer.

640

641

642

643 **Table 1:** Summary of *B. coagulans* B-768 assembly and comparison with reference genomes

Features	**B-768**	**36D1**	**DSM1**
Length (bp)	3,944,476	3,552,226	3,366,995
G+C Content (%)	45.7	46.0	46.5
CDS	3,863	3,227	3,215
ncRNA	4	5	7
rRNA	30	30	30
tRNA	85	84	84
CRISPR arrays	5	4	3

644

645 **Table 2:** Number of genes in restriction-modification (RM) systems

R-M	**B-768**	**36D1*(31)***	**DSM1*(31)***
Type I	7	19	6
Type II	2	0	1
Type III	0	2	2
Type IV	2	3	3
Total	**11**	**24**	**12**

646

647 **Table 3:** Identification of spacers in B-768 CRISPR arrays

Spacer	Hit ID	Genus	Type	Method
GGTTGGTGTAGCCGGTTGATATTCCTGATTAATCAA	JQ362498.1	*Sphingomonas*	Phage	SpacePHARER
GGTTGGTGTAGCCGGTTGATATTCCTGATTAATCAA	KC481682.1	*Bacillus*	Phage	SpacePHARER
GCTTTTAAACTCCATCAGTGGTTTTTATTTTTGGGT	KX965989.1	*Aeribacillus*	Phage	SpacePHARER
TATAGAAACCACGTTTTCGGCGACAAGCCTGGCATTG	KU665491.1	*Bacillus*	Phage	SpacePHARER
ATCCCGGCGGTGCTGGCCTATGTCGGAAAATATGC	NZ_CP022365.1	*Azospirillum*	Plasmid	Blastn_short
CTTTAAAAAAATCACAAAATGGAAAAATTTACGTGCGGAATATGCGCGAAATCATATTCAACTCCAACTGTCAT	NZ_CP075898.1	*Exiguobacterium*	Plasmid	Blastn_short
AAAACTAAGTTAAAAAAGAATTTAGCCGGTATGGCC	NZ_CP015595.1	*Acinetobacter*	Plasmid	Blastn_short
TGAAACCGCGGGAAAGCCAATACGGCGGCGAACCA	NZ_CP032924.1	*Agrobacterium*	Plasmid	Blastn_short
GCGATATACTGCCGTAGGGCATCGTCGCCGTCAATAAA	NZ_CP024924.1	*Sphingomonas*	Plasmid	Blastn_short

648

649 **Table 4:** BLASTp top hits for B-768 xylosidase proteins

Query	Subject	Description	Organism	Query Cover	E-value	Per. Identity
Alpha-xylosidase	WP_063613105.1	alpha-xylosidase	*Bacillus sp.*	1	0	0.9894
Beta-xylosidase/AraC-like DNA-binding protein	WP_161788365.1	helix-turn-helix domain-containing protein	*Bacillus coagulans*	1	0	0.9805
GH43 family beta-xylosidase	WP_071451997.1	family 43 glycosyl hydrolase	*Bacillus coagulans*	1	0	0.9574
4-beta-xylosidase	WP_014868562.1	glycoside hydrolase family 43 protein	*Melissococcus plutonius*	0.98	0	0.6485

650

651 **Table 5:** Differential protein expression for candidate proteins contributing to cellular robustness

652 of B-768 growing in SGH

Protein ID	Function	Class	Log_2-fold Change	q-value
Ga0586967_01_1426112_1427749	methyl-accepting chemotaxis protein	Chemotaxis	7.21	2.2E-14
Ga0586967_01_2953390_2954649	methyl-accepting chemotaxis protein	Chemotaxis	2.1	0.00377
Ga0586967_01_1922219_1923952	methyl-accepting chemotaxis protein	Chemotaxis	2.02	0.0171
Ga0586967_01_3602104_3603432	methyl-accepting chemotaxis protein	Chemotaxis	-6.24	0.00197
Ga0586967_01_1885126_1886544	PTS system trehalose-specific IIC component	Transport	-1.06	0.0103
Ga0586967_01_1886575_1887057	PTS system glucose-specific IIA component	Transport	-1.18	0.00121
Ga0586967_01_1467232_1467561	PTS system cellobiose-specific IIA component	Transport	-1.38	0.00901
Ga0586967_01_1541669_1542151	fructoselysine and glucoselysine-specific PTS system IIB component	Transport	-2.64	0.0316
Ga0586967_01_2529421_2529912	mannose/fructose/N-acetylgalactosamine-specific phosphotransferase system component IIB	Transport	-3.63	0.00023
Ga0586967_01_1189660_1191024	PTS system ascorbate-specific IIC component	Transport	-3.89	9.7E-10
Ga0586967_01_1452905_1453891	LacI family transcriptional regulator	Regulator	7.71	2.2E-14
Ga0586967_01_1692988_1693203	putative transcriptional regulator	Regulator	5.56	0.00345
Ga0586967_01_633467_634027	TetR/AcrR family transcriptional repressor of lmrAB and yxaGH operons	Regulator	3.97	0.00309
Ga0586967_01_3908323_3909216	phenylacetic acid degradation operon negative regulatory protein	Regulator	3.62	0.0132
Ga0586967_01_2622621_2623172	DNA-binding transcriptional ArsR family regulator	Regulator	3.09	0.00232
Ga0586967_01_1173785_1174315	DNA-binding MarR family transcriptional regulator	Regulator	2.63	0.0019

Ga0586967_01_3081124_3082011	DNA-binding transcriptional LysR family regulator	Regulator	2.27	9.3E-10
Ga0586967_01_3363633_3364772	GntR family transcriptional regulator of arabinose operon	Regulator	2.03	7.9E-10
Ga0586967_01_1915388_1915990	AcrR family transcriptional regulator	Regulator	-3.24	0.00012
Ga0586967_01_3584855_3586105	DNA-binding transcriptional ArsR family regulator	Regulator	-4.86	8.4E-08

653

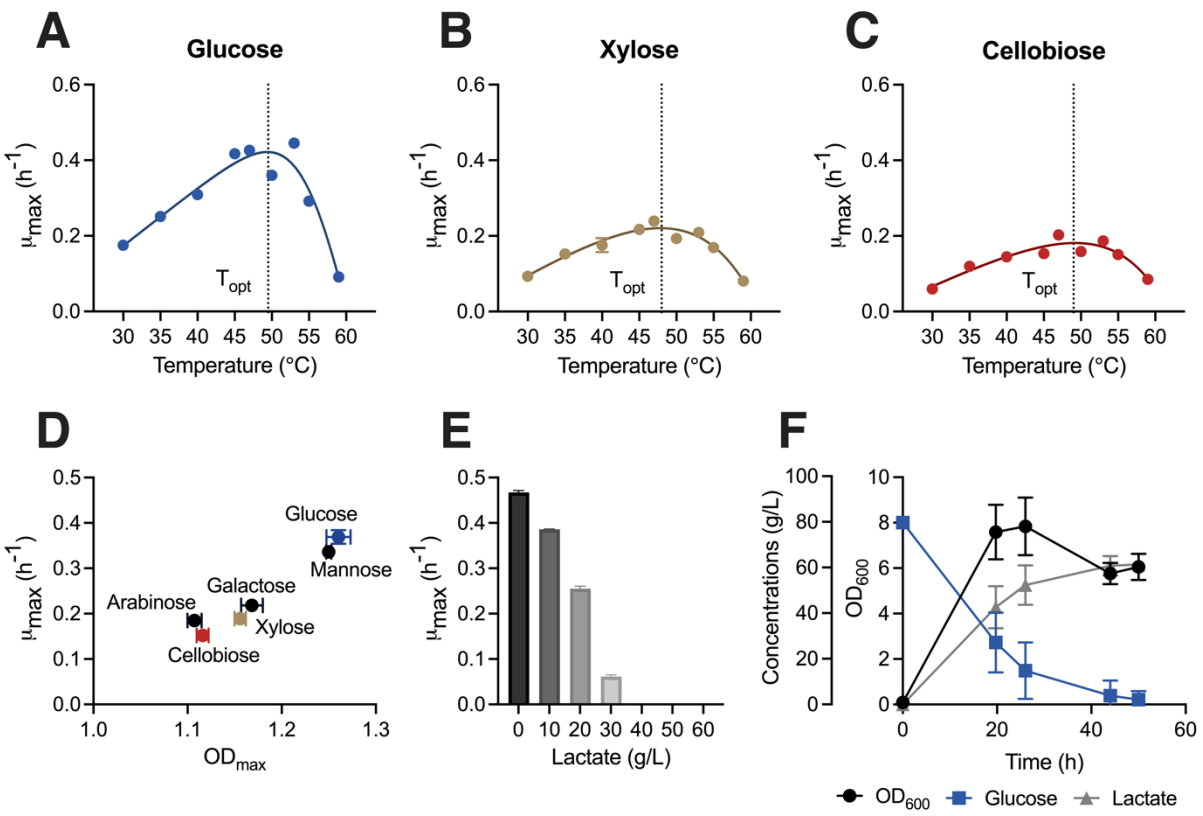

654

655 **Figure 1:** Physiological characterization of *B. coagulans* B-768 reveals cellular robustness and
656 efficient utilization of various carbon sources at various temperatures. (A–C) Dependence of
657 specific growth rates of B-768 on temperatures when grown on (A) glucose, (B) xylose, and (C)
658 cellobiose. (D) Carrying capacity and maximum specific growth rate of B-768 growing on various
659 C5, C6, and C12 fermentable sugars at 50 °C. (E) Effect of lactate concentrations on maximum
660 specific growth rates of B-768 growing on glucose at 50 °C. (F) Kinetic profiles of cell growth,
661 glucose consumption, and lactate production in a pH-controlled bioreactor at 50 °C. Data points
662 represent 1 mean ± 1 standard deviation of three biological replicates.

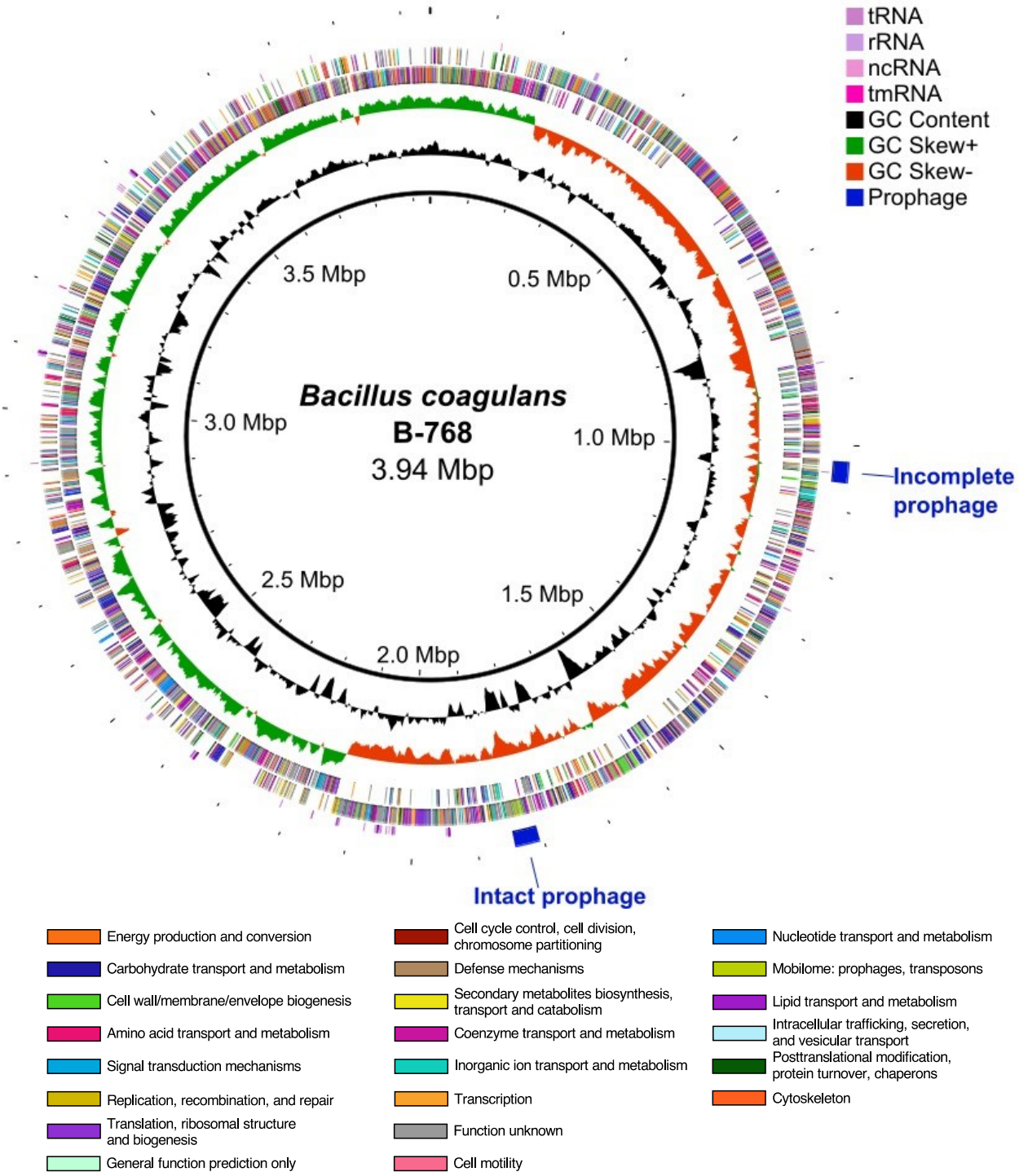

Figure 2: Circular genome map of *Bacillus coagulans* B-768. Tracks from outside to in are as follows: PHASTEST 3.0 prophage regions, non-coding RNAs, forward and reverse strand CDS colored by COG category, GC Skew = (G - C)/(G + C), and GC content. Abbreviations: tRNA,

667 transfer RNA; rRNA, ribosomal RNA; ncRNA, non-coding RNA; tmRNA, transfer-messenger

668 RNA.

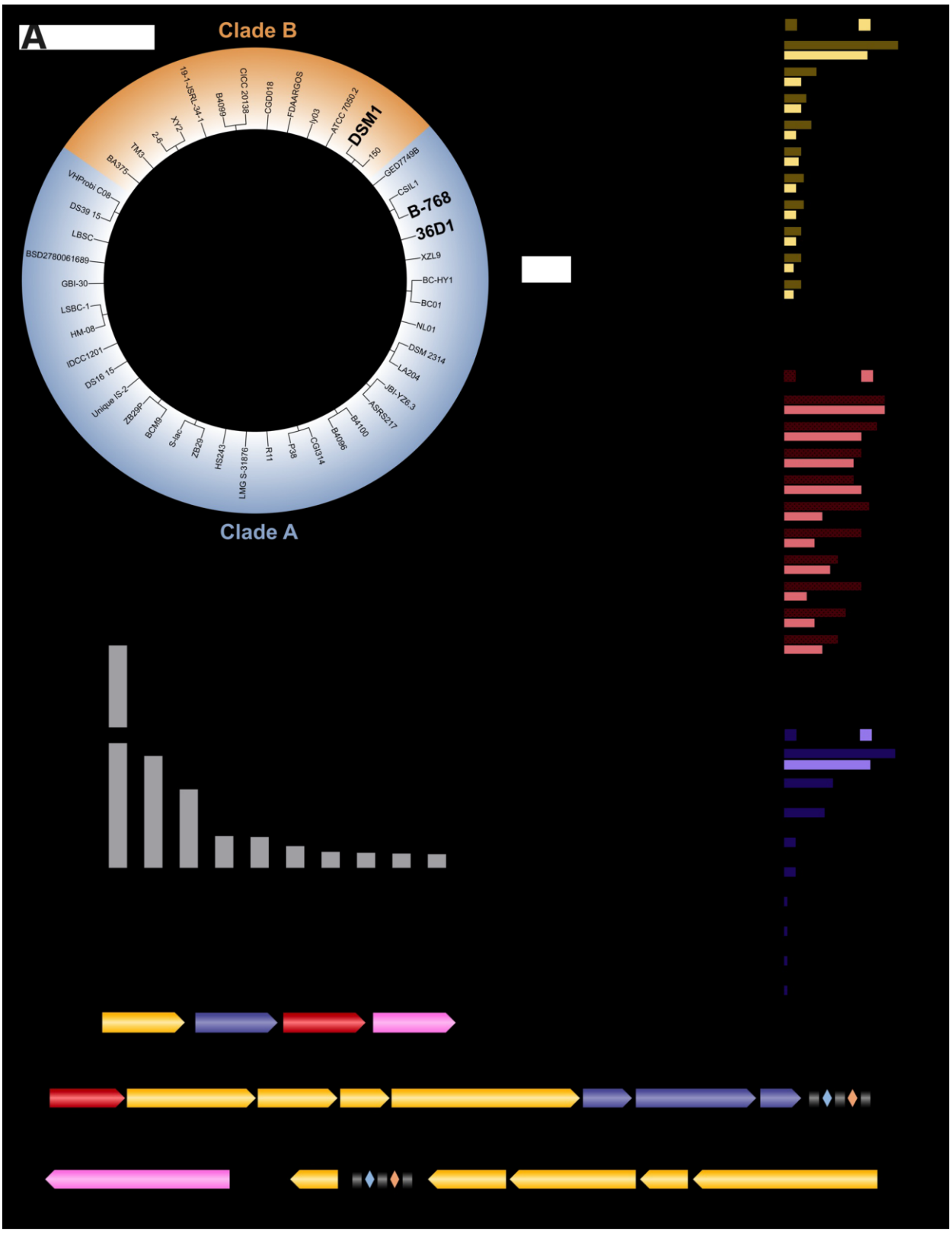
A
Clade B
19-1-ISRL-34-1
CICC 20138
CGD018
FDAARGOS
ATCC 7060.2
DSM1
150
GED7749B
CSIL1
B-768
36D1
XZL9
BC-HY1
BC01
NL01
DSM 2314
LA204
JBI-YZ6.3
ASRS217
B4100
BA096
CGI314
P38
R11
LMG S-31876
HS243
ZB29
S-lac
BCM9
ZB29P
Unique IS-2
DS16 15
IDCC1201
HM-08
LSBC-1
GBI-30
BSD2780061689
LBSC
DS39 15
VHProbi C08
BA375
TM3
2-6
XY2
BA099
Clade A

669

670 **Figure 3:** Comparative and functional genomics of *B. coagulans* B-768. (A) Core genome
671 alignment of *B. coagulans* pan-genome (n = 55). (B) Percent change of COG categories between
672 strains B-768 and 36D1. Numbers above the bars indicate the excess number of proteins in B-768
673 relative to 36D1. Full COG Category names are listed at the end of the figure caption. (C–E)
674 Breakdown of most abundant proteins in (C) Carbohydrate Metabolism and Transport, (D)
675 Transcription, and (E) Mobilome COG categories. (F) Predicted CRISPR-Cas operons of B-768.
676 COG Categories: U = Intracellular Trafficking, Secretion, and Vesicular Transport; X =
677 Mobilome; G = Carbohydrate Transport and Metabolism; Q = Secondary Metabolites
678 Biosynthesis, Transport and Catabolism; K = Transcription; I = Lipid Transport and Metabolism;
679 M = Cell Wall/Membrane/Envelope Biogenesis; D = Cell Cycle Control, Cell Division,
680 Chromosome Partitioning; H = Coenzyme Transport and Metabolism; C = Energy Production and
681 Conversion.

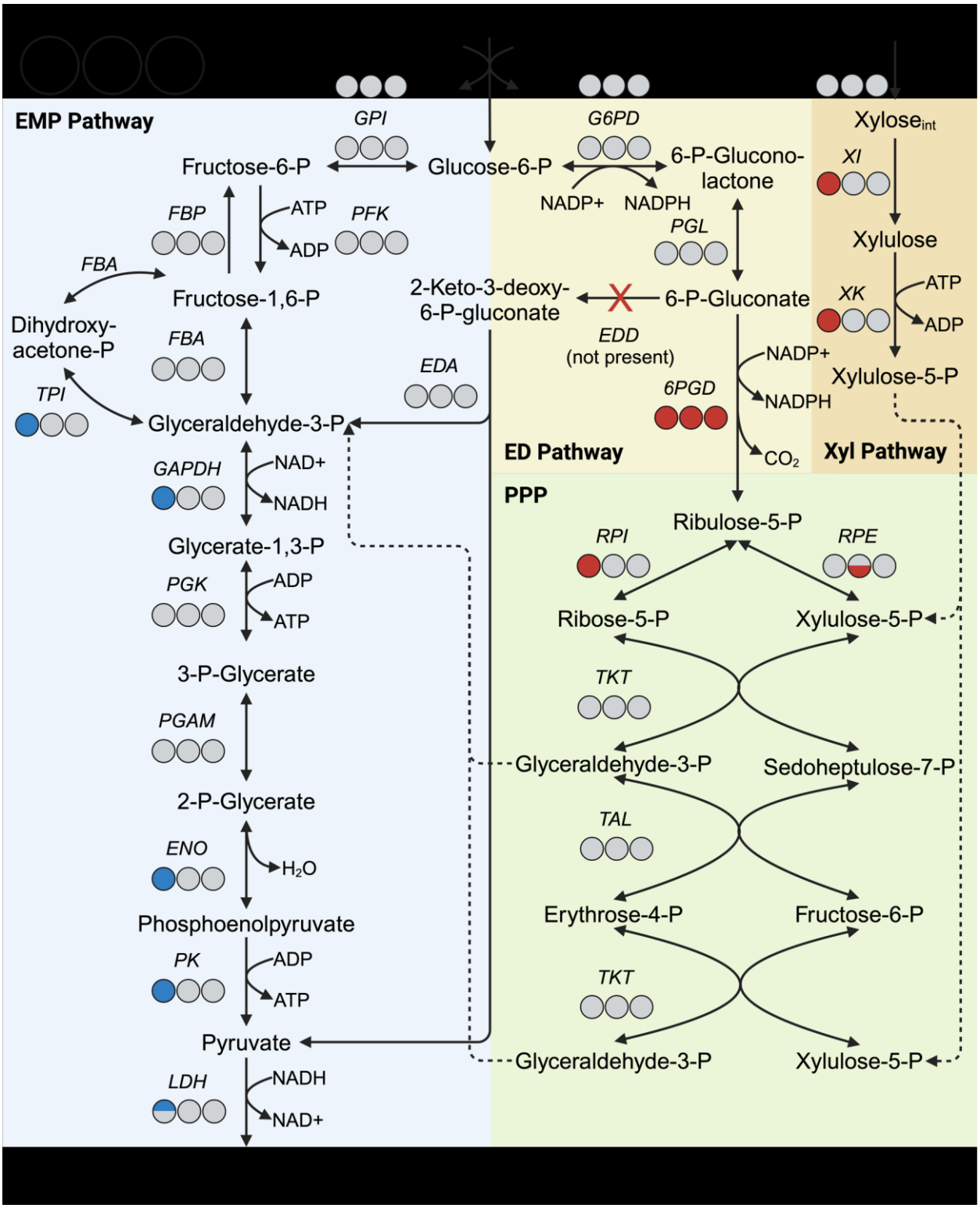

682

683 **Figure 4:** Central carbon metabolism of B-768. Circles from left to right represent the differential

684 expression of a given protein in 1.) xylose vs. glucose, 2.) xylose and glucose mixture vs. glucose,

685 and 3.) switchgrass hydrolysate vs. glucose conditions. Red = upregulated with $\log_2$-fold change
686 ≥ 1 and $q < 0.05$; Blue = downregulated with $\log_2$-fold change ≤ -1 and $q < 0.05$; Grey = Not
687 Significant. Paralogs of the same enzyme were plotted as half circles with the most abundant
688 paralog on top.

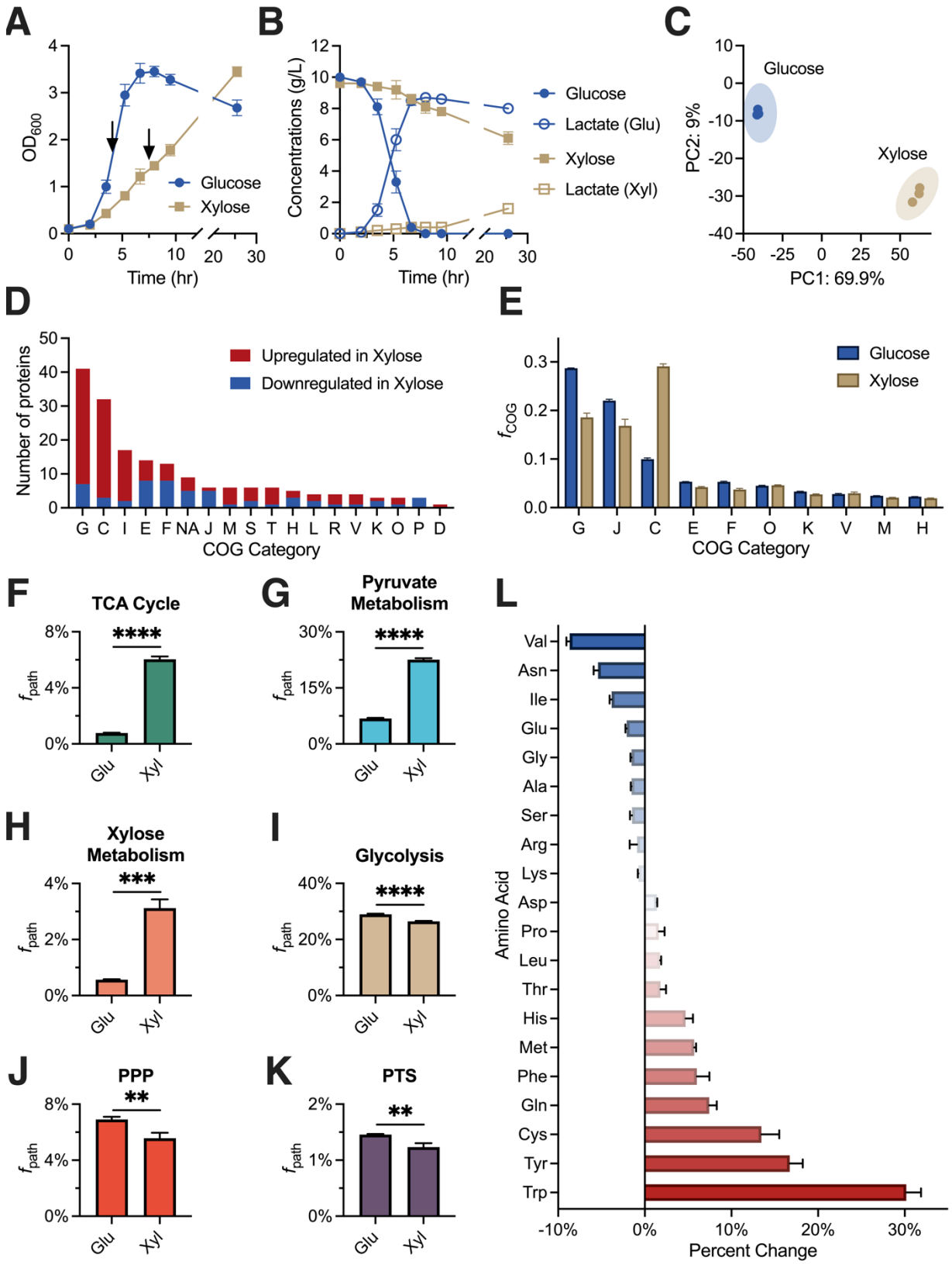
A
OD600
Time (hr)
Glucose
Xylose
B
Concentrations (g/L)
Time (hr)
Glucose
Lactate (Glu)
Xylose
Lactate (Xyl)
C
PC2: 9%
PC1: 69.9%
Glucose
Xylose
D
Number of proteins
Upregulated in Xylose
Downregulated in Xylose
G C I E F NA J M S T H L R V K O P D
COG Category
E
fCOG
Glucose
Xylose
G J C E F O K V M H
COG Category
F
TCA Cycle
fpath
****
Glu Xyl
G
Pyruvate Metabolism
fpath
****
Glu Xyl
H
Xylose Metabolism
fpath
***
Glu Xyl
I
Glycolysis
fpath
****
Glu Xyl
J
PPP
fpath
**
Glu Xyl
K
PTS
fpath
**
Glu Xyl
L
Amino Acid
Val
Asn
Ile
Glu
Gly
Ala
Ser
Arg
Lys
Asp
Pro
Leu
Thr
His
Met
Phe
Gln
Cys
Tyr
Trp
Percent Change

689

690 **Figure 5:** *B. coagulans* B-768 exhibited distinct proteomes for growing on glucose and xylose.
691 (A–B) Kinetic profiles of (A) cell growth and (B) glucose/xylose consumption and lactate
692 production. Proteomics samples were collected from parallel cultures at the time points indicated
693 by black arrows. (C) Principal component analysis of *B. coagulans* B-768 proteomes for growth
694 on glucose and xylose. (D) Number of differentially expressed proteins between glucose and
695 xylose conditions for most perturbed COG categories. (E) Mass fraction of proteomes in top COG
696 categories (f_{COG}) for glucose and xylose conditions. (F–K) Proteome allocation by pathway for
697 glucose and xylose conditions. (L) Percent change in amino acid allocation of proteomes between
698 glucose and xylose conditions. COG Categories: G = Carbohydrate Transport and Metabolism; C
699 = Energy Production and Conversion; I = Lipid Transport and Metabolism; E = Amino Acid
700 Transport and Metabolism; F = Nucleotide Transport and Metabolism; NA = No COG annotation;
701 J = Translation; M = Cell Wall/Membrane/Envelope Biogenesis; S = Function Unknown; T =
702 Signal Transduction Mechanisms; H = Coenzyme Transport and Metabolism; L = Replication,
703 Recombination, and Repair; R = General Function Prediction Only; V = Defense Mechanisms; K
704 = Transcription; O = Posttranslation Modification, Protein Turnover, Chaperones; P = Inorganic
705 Ion Transport and Metabolism; D = Cell Cycle Control, Cell Division, Chromosome Partitioning.
706 Statistics for F–K were performed using an unpaired t-test with default settings in GraphPad Prism
707 v10.2.3. Error bars represent the standard deviation of 3 biological replicates. **** = p-value <
708 0.0001; *** = p-value < 0.001; ** = p-value < 0.01.

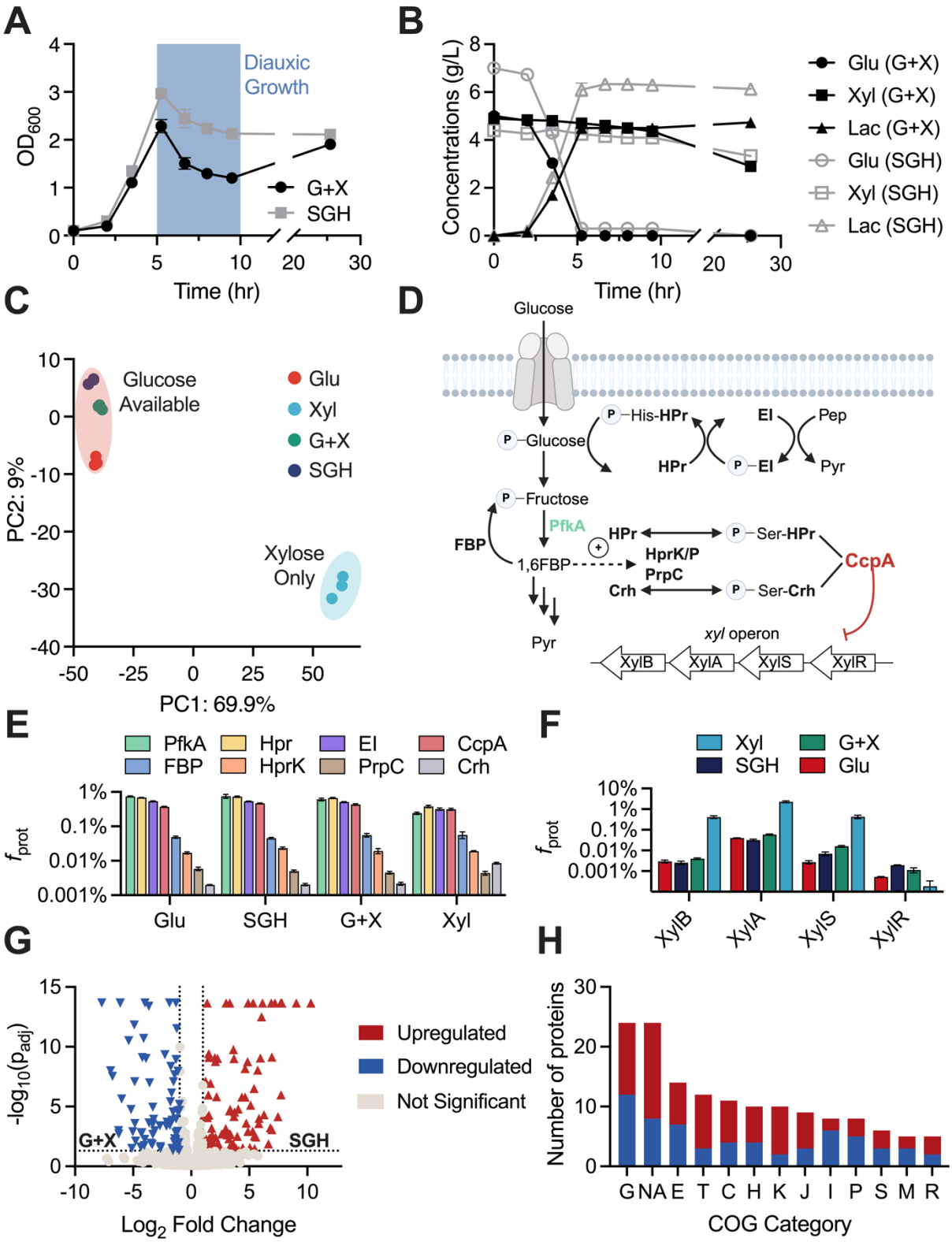
A
Diauxic Growth
OD600
Time (hr)
G+X
SGH
B
Concentrations (g/L)
Time (hr)
Glu (G+X)
Xyl (G+X)
Lac (G+X)
Glu (SGH)
Xyl (SGH)
Lac (SGH)
C
Glucose Available
Xylose Only
Glu
Xyl
G+X
SGH
PC2: 9%
PC1: 69.9%
D
Glucose
His-HPr
EI
Pep
Glucose
HPr
EI
Pyr
Fructose
PfkA
FBP
HPr
Ser-HPr
1,6FBP
HprK/P
PrpC
CcpA
Crh
Ser-Crh
Pyr
xyl operon
XylB
XylA
XylS
XylR
E
PfkA
FBP
Hpr
HprK
EI
PrpC
CcpA
Crh
fprot
Glu
SGH
G+X
Xyl
F
Xyl
SGH
G+X
Glu
fprot
XylB
XylA
XylS
XylR
G
-log10(padj)
G+X
SGH
Log2 Fold Change
Upregulated
Downregulated
Not Significant
H
Number of proteins
G N A E T C H K J I P S M R
COG Category

709

710 **Figure 6:** Growth of B-768 in refined sugars and raw hydrolysate reveals mechanisms of cellular
711 robustness and carbon catabolite repression. (A) Growth profiles of B-768 grown on glucose +
712 xylose (G+X) mixture and switchgrass hydrolysate (SGH). (B) Glucose and xylose consumption
713 and lactate production profiles of B-768 grown on G+X and SGH. (C) Principal component
714 analysis plot of B-768 proteomes grown on different sugars. (D) Schematic of CCR in *Bacillus*
715 species. (E) Levels of CCR proteins in B-768 proteomes grown on different sugars. (F) Levels of
716 *xyl* proteins in B-768 proteomes grown on different sugars. (G) Volcano plot of differentially
717 expressed proteins between SGH and G+X conditions. (H) Number of significantly perturbed
718 proteins by COG category. COG Categories: G = Carbohydrate Transport and Metabolism; E =
719 Amino Acid Transport and Metabolism; T = Signal Transduction Mechanisms; C = Energy
720 Production and Conversion; H = Coenzyme Transport and Metabolism; NA = No COG annotation;
721 K = Transcription; J = Translation; I = Lipid Transport and Metabolism; P = Inorganic Ion
722 Transport and Metabolism; S = Function Unknown; M = Cell Wall/Membrane/Envelope
723 Biogenesis; R = General Function Prediction Only.

References

1. Lynd LR, Beckham GT, Guss AM, Jayakody LN, Karp EM, Maranas C, McCormick RL, Amador-Noguez D, Bomble YJ, Davison BH, Trinh CT. 2022. Toward low-cost biological and hybrid biological/catalytic conversion of cellulosic biomass to fuels. Energy & Environmental Science 15:938-990.
2. Ragauskas AJ, Williams CK, Davison BH, Britovsek G, Cairney J, Eckert CA, Frederick WJ, Jr., Hallett JP, Leak DJ, Liotta CL, Mielenz JR, Murphy R, Templer R, Tschaplinski T. 2006. The path forward for biofuels and biomaterials. Science (New York, NY) 311:484-489.
3. Langholtz MH. 2024. 2023 Billion-Ton Report.
4. Zoghlami A, Paës G. 2019. Lignocellulosic biomass: understanding recalcitrance and predicting hydrolysis. Frontiers in chemistry 7:874.
5. Lee J-W, Trinh CT. 2020. Towards renewable flavors, fragrances, and beyond. Current Opinion in Biotechnology 61:168-180.
6. Bond JQ, Upadhye AA, Olcay H, Tompsett GA, Jae J, Xing R, Alonso DM, Wang D, Zhang T, Kumar R. 2014. Production of renewable jet fuel range alkanes and commodity chemicals from integrated catalytic processing of biomass. Energy & Environmental Science 7:1500-1523.
7. Holbery J, Houston D. 2006. Natural-fiber-reinforced polymer composites in automotive applications. Jom 58:80-86.
8. Lee JW, Na D, Park JM, Lee J, Choi S, Lee SY. 2012. Systems metabolic engineering of microorganisms for natural and non-natural chemicals. Nature chemical biology 8:536-546.

747 9. Keasling J, Chou H. 2008. Metabolic engineering delivers next-generation biofuels. Nat
748 Biotechnol 26:298 - 299.
749 10. Napora-Wijata K, Strohmeier GA, Winkler M. 2014. Biocatalytic reduction of carboxylic
750 acids. Biotechnology journal 9:822-843.
751 11. Trinh CT, Unrean P, Srienc F. 2008. Minimal Escherichia coli cell for the most efficient
752 production of ethanol from hexoses and pentoses. Applied and environmental microbiology
753 74:3634-3643.
754 12. Weber C, Farwick A, Benisch F, Brat D, Dietz H, Subtil T, Boles E. 2010. Trends and
755 challenges in the microbial production of lignocellulosic bioalcohol fuels. Applied
756 microbiology and biotechnology 87:1303-1315.
757 13. Lynd LR, Liang X, Biddy MJ, Allee A, Cai H, Foust T, Himmel ME, Laser MS, Wang M,
758 Wyman CE. 2017. Cellulosic ethanol: status and innovation. Current opinion in
759 biotechnology 45:202-211.
760 14. Kunjapur AM, Prather KL. 2015. Microbial engineering for aldehyde synthesis. Applied and
761 Environmental Microbiology 81:1892-1901.
762 15. Yuzawa S, Mirsiaghi M, Jocic R, Fujii T, Masson F, Benites VT, Baidoo EE, Sundstrom E,
763 Tanjore D, Pray TR. 2018. Short-chain ketone production by engineered polyketide
764 synthases in Streptomyces albus. Nature communications 9:4569.
765 16. Kim DI, Chae TU, Kim HU, Jang WD, Lee SY. 2021. Microbial production of multiple
766 short-chain primary amines via retrobiosynthesis. Nature Communications 12:173.
767 17. Layton DS, Trinh CT. 2014. Engineering modular ester fermentative pathways in
768 *Escherichia coli*. Metabolic engineering 26:77-88.

769 18. Thompson RA, Trinh CT. 2014. Enhancing fatty acid ethyl ester production in
770 Saccharomyces cerevisiae through metabolic engineering and medium optimization.
771 Biotechnology and bioengineering 111:2200-2208.
772 19. Anjum A, Zuber M, Zia KM, Noreen A, Anjum MN, Tabasum S. 2016. Microbial production
773 of polyhydroxyalkanoates (PHAs) and its copolymers: A review of recent advancements.
774 International journal of biological macromolecules 89:161-174.
775 20. Cappello J. 1990. The biological production of protein polymers and their use. Trends in
776 biotechnology 8:309-311.
777 21. Ubando AT, Felix CB, Chen W-H. 2020. Biorefineries in circular bioeconomy: A
778 comprehensive review. Bioresource technology 299:122585.
779 22. Almeida JR, Modig T, Petersson A, Hähn-Hägerdal B, Lidén G, Gorwa-Grauslund MF.
780 2007. Increased tolerance and conversion of inhibitors in lignocellulosic hydrolysates by
781 Saccharomyces cerevisiae. Journal of Chemical Technology & Biotechnology: International
782 Research in Process, Environmental & Clean Technology 82:340-349.
783 23. Wang S, Sun X, Yuan Q. 2018. Strategies for enhancing microbial tolerance to inhibitors for
784 biofuel production: a review. Bioresource technology 258:302-309.
785 24. Chubukov V, Gerosa L, Kochanowski K, Sauer U. 2014. Coordination of microbial
786 metabolism. Nature Reviews Microbiology 12:327-340.
787 25. Stephanopoulos G. 2007. Challenges in Engineering Microbes for Biofuels Production.
788 Science 315:801-804.
789 26. Zheng Z, Lin X, Jiang T, Ye W, Ouyang J. 2016. Genomic analysis of a xylose operon and
790 characterization of novel xylose isomerase and xylulokinase from Bacillus coagulans NL01.
791 Biotechnology letters 38:1331-1339.

792 27. Zheng Z, Jiang T, Zou L, Ouyang S, Zhou J, Lin X, He Q, Wang L, Yu B, Xu H. 2018.
793 Simultaneous consumption of cellobiose and xylose by Bacillus coagulans to circumvent
794 glucose repression and identification of its cellobiose-assimilating operons. Biotechnology
795 for biofuels 11:320.
796 28. Yao K, Zhou Q-x, Liu D-m, Chen S-m, Yuan K. 2019. Comparative proteomics of the
797 metabolic pathways involved in l-lactic acid production in Bacillus coagulans BCS13002
798 using different carbon sources. LWT 116:108445.
799 29. Aulitto M, Fusco S, Bartolucci S, Franzén CJ, Contursi P. 2017. Bacillus coagulans MA-13:
800 a promising thermophilic and cellulolytic strain for the production of lactic acid from
801 lignocellulosic hydrolysate. Biotechnology for biofuels 10:1-15.
802 30. Aulitto M, Fusco S, Nickel DB, Bartolucci S, Contursi P, Franzén CJ. 2019. Seed culture
803 pre-adaptation of Bacillus coagulans MA-13 improves lactic acid production in simultaneous
804 saccharification and fermentation. Biotechnology for biofuels 12:1-11.
805 31. Su F, Xu P. 2014. Genomic analysis of thermophilic Bacillus coagulans strains: efficient
806 producers for platform bio-chemicals. Scientific reports 4:3926.
807 32. Riazi S, Wirawan R, Badmaev V, Chikindas M. 2009. Characterization of lactosporin, a
808 novel antimicrobial protein produced by Bacillus coagulans ATCC 7050. Journal of applied
809 microbiology 106:1370-1377.
810 33. Marrec L. 1998. Coagulin, a bacteriocin-like inhibitory substance produced by Bacillus
811 coagulans I4. Journal of applied microbiology 85:42-50.
812 34. Khatri I, Sharma S, Ramya T, Subramanian S. 2016. Complete genomes of Bacillus
813 coagulans S-lac and Bacillus subtilis TO-A JPC, two phylogenetically distinct probiotics.
814 PLoS One 11:e0156745.

815 35. De Clerck E, Rodriguez-Diaz M, Forsyth G, Lebbe L, Logan NA, DeVos P. 2004. Polyphasic
816 characterization of Bacillus coagulans strains, illustrating heterogeneity within this species,
817 and emended description of the species. Systematic and applied microbiology 27:50-60.
818 36. Patel MA, Ou MS, Harbrucker R, Aldrich HC, Buszko ML, Ingram LO, Shanmugam K.
819 2006. Isolation and characterization of acid-tolerant, thermophilic bacteria for effective
820 fermentation of biomass-derived sugars to lactic acid. Applied and Environmental
821 Microbiology 72:3228-3235.
822 37. Patel MA, Ou MS, Ingram LO, Shanmugam K. 2005. Simultaneous saccharification and co-
823 fermentation of crystalline cellulose and sugar cane bagasse hemicellulose hydrolysate to
824 lactate by a thermotolerant acidophilic Bacillus sp. Biotechnology progress 21:1453-1460.
825 38. Ouyang J, Cai C, Chen H, Jiang T, Zheng Z. 2012. Efficient non-sterilized fermentation of
826 biomass-derived xylose to lactic acid by a thermotolerant Bacillus coagulans NL01. Applied
827 biochemistry and biotechnology 168:2387-2397.
828 39. Ahorsu R, Cintorrino G, Medina F, Constantí M. 2019. Microwave processes: a viable
829 technology for obtaining xylose from walnut shell to produce lactic acid by Bacillus
830 coagulans. Journal of cleaner production 231:1171-1181.
831 40. Wishart DS, Han S, Saha S, Oler E, Peters H, Grant JR, Stothard P, Gautam V. 2023.
832 PHASTEST: faster than PHASTER, better than PHAST. Nucleic Acids Research 51:W443-
833 W450.
834 41. Shimoyama Y. 2022. COGclassifier: A tool for classifying prokaryote protein sequences into
835 COG functional category, vv1.0.5. GitHub, https://github.com/moshi4/COGclassifier.
836 42. Swint-Kruse L, Matthews KS. 2009. Allostery in the LacI/GalR family: variations on a
837 theme. Current opinion in microbiology 12:129-137.

838 43. Maddocks SE, Oyston PC. 2008. Structure and function of the LysR-type transcriptional
839 regulator (LTTR) family proteins. Microbiology 154:3609-3623.
840 44. Hoskisson PA, Rigali S. 2009. Variation in form and function: the helix-turn-helix regulators
841 of the GntR superfamily. Advances in applied microbiology 69:1-22.
842 45. Busenlehner LS, Pennella MA, Giedroc DP. 2003. The SmtB/ArsR family of
843 metalloregulatory transcriptional repressors: structural insights into prokaryotic metal
844 resistance. FEMS microbiology reviews 27:131-143.
845 46. Pei Z, Sadiq FA, Han X, Zhao J, Zhang H, Ross RP, Lu W, Chen W. 2021. Comprehensive
846 scanning of prophages in Lactobacillus: distribution, diversity, antibiotic resistance genes,
847 and linkages with CRISPR-Cas systems. Msystems 6:10.1128/msystems. 01211-20.
848 47. Bondy-Denomy J, Qian J, Westra ER, Buckling A, Guttman DS, Davidson AR, Maxwell
849 KL. 2016. Prophages mediate defense against phage infection through diverse mechanisms.
850 The ISME journal 10:2854-2866.
851 48. Salvetti E, Orrù L, Capozzi V, Martina A, Lamontanara A, Keller D, Cash H, Felis GE,
852 Cattivelli L, Torriani S. 2016. Integrate genome-based assessment of safety for probiotic
853 strains: Bacillus coagulans GBI-30, 6086 as a case study. Applied microbiology and
854 biotechnology 100:4595-4605.
855 49. Saroj DB, Gupta AK. 2020. Genome based safety assessment for Bacillus coagulans strain
856 LBSC (DSM 17654) for probiotic application. International journal of food microbiology
857 318:108523.
858 50. Samson JE, Moineau S. 2013. Bacteriophages in food fermentations: new frontiers in a
859 continuous arms race. Annual review of food science and technology 4:347-368.

860 51. Roberts RJ, Belfort M, Bestor T, Bhagwat AS, Bickle TA, Bitinaite J, Blumenthal RM,
861 Degtyarev SK, Dryden DT, Dybvig K. 2003. A nomenclature for restriction enzymes, DNA
862 methyltransferases, homing endonucleases and their genes. Nucleic acids research 31:1805-
863 1812.
864 52. Mojica FJ, Díez-Villaseñor Cs, García-Martínez J, Soria E. 2005. Intervening sequences of
865 regularly spaced prokaryotic repeats derive from foreign genetic elements. Journal of
866 molecular evolution 60:174-182.
867 53. Karginov FV, Hannon GJ. 2010. The CRISPR system: small RNA-guided defense in bacteria
868 and archaea. Molecular cell 37:7-19.
869 54. Al-Shayeb B, Sachdeva R, Chen L-X, Ward F, Munk P, Devoto A, Castelle CJ, Olm MR,
870 Bouma-Gregson K, Amano Y. 2020. Clades of huge phages from across Earth's ecosystems.
871 Nature 578:425-431.
872 55. Kraus A, Hueck C, Gärtner D, Hillen W. 1994. Catabolite repression of the Bacillus subtilis
873 xyl operon involves a cis element functional in the context of an unrelated sequence, and
874 glucose exerts additional xylR-dependent repression. Journal of bacteriology 176:1738-
875 1745.
876 56. Dahl MK, Schmiedel D, Hillen W. 1995. Glucose and glucose-6-phosphate interaction with
877 Xyl repressor proteins from Bacillus spp. may contribute to regulation of xylose utilization.
878 Journal of bacteriology 177:5467-5472.
879 57. Walton SL, Bischoff KM, van Heiningen AR, van Walsum GP. 2010. Production of lactic
880 acid from hemicellulose extracts by Bacillus coagulans MXL-9. Journal of Industrial
881 Microbiology and Biotechnology 37:823-830.

882 58. Kandler O. 1983. Carbohydrate metabolism in lactic acid bacteria. Antonie van
883 Leeuwenhoek 49:209-224.
884 59. Gu Y, Ding Y, Ren C, Sun Z, Rodionov DA, Zhang W, Yang S, Yang C, Jiang W. 2010.
885 Reconstruction of xylose utilization pathway and regulons in Firmicutes. BMC genomics
886 11:1-14.
887 60. Ong SA, Ng ZJ, Wu JC. 2016. Production of high concentration of L-lactic acid from
888 cellobiose by thermophilic Bacillus coagulans WCP10-4. Applied microbiology and
889 biotechnology 100:6501-6508.
890 61. Sternberg D, Vuayakumar P, Reese E. 1977. β-Glucosidase: microbial production and effect
891 on enzymatic hydrolysis of cellulose. Canadian Journal of Microbiology 23:139-147.
892 62. Frey PA. 1996. The Leloir pathway: a mechanistic imperative for three enzymes to change
893 the stereochemical configuration of a single carbon in galactose. The FASEB Journal 10:461-
894 470.
895 63. Sun T, Altenbuchner J. 2010. Characterization of a mannose utilization system in Bacillus
896 subtilis. Journal of bacteriology 192:2128-2139.
897 64. Seo H, Giannone RJ, Yang Y-H, Trinh CT. 2022. Proteome reallocation enables the selective
898 de novo biosynthesis of non-linear, branched-chain acetate esters. Metabolic Engineering
899 73:38-49.
900 65. Akashi H, Gojobori T. 2002. Metabolic efficiency and amino acid composition in the
901 proteomes of Escherichia coli and Bacillus subtilis. Proceedings of the National Academy of
902 Sciences 99:3695-3700.
903 66. Görke B, Stülke J. 2008. Carbon catabolite repression in bacteria: many ways to make the
904 most out of nutrients. Nature Reviews Microbiology 6:613-624.

905 67. Galinier A, Haiech J, Kilhoffer M-C, Jaquinod M, Stülke J, Deutscher J, Martin-Verstraete
906 I. 1997. The Bacillus subtilis crh gene encodes a HPr-like protein involved in carbon
907 catabolite repression. Proceedings of the National Academy of Sciences 94:8439-8444.
908 68. Galinier A, Kravanja M, Engelmann R, Hengstenberg W, Kilhoffer M-C, Deutscher J,
909 Haiech J. 1998. New protein kinase and protein phosphatase families mediate signal
910 transduction in bacterial catabolite repression. Proceedings of the National Academy of
911 Sciences 95:1823-1828.
912 69. Deutscher J, Küster E, Bergstedt U, Charrier V, Hillen W. 1995. Protein kinase-dependent
913 HPr/CcpA interaction links glycolytic activity to carbon catabolite repression in Gram-
914 positive bacteria. Molecular microbiology 15:1049-1053.
915 70. Schumacher MA, Seidel G, Hillen W, Brennan RG. 2007. Structural mechanism for the fine-
916 tuning of CcpA function by the small molecule effectors glucose 6-phosphate and fructose
917 1, 6-bisphosphate. Journal of molecular biology 368:1042-1050.
918 71. Seidel G, Diel M, Fuchsbauer N, Hillen W. 2005. Quantitative interdependence of
919 coeffectors, CcpA and cre in carbon catabolite regulation of Bacillus subtilis. The FEBS
920 journal 272:2566-2577.
921 72. Singh KD, Schmalisch MH, Stülke Jr, Görke B. 2008. Carbon catabolite repression in
922 Bacillus subtilis: quantitative analysis of repression exerted by different carbon sources.
923 Journal of Bacteriology 190:7275-7284.
924 73. Klinke HB, Thomsen A, Ahring BK. 2004. Inhibition of ethanol-producing yeast and
925 bacteria by degradation products produced during pre-treatment of biomass. Applied
926 microbiology and biotechnology 66:10-26.

927 74. Pienkos PT, Zhang M. 2009. Role of pretreatment and conditioning processes on toxicity of
928 lignocellulosic biomass hydrolysates. Cellulose 16:743-762.
929 75. Ujor VC, Okonkwo CC. 2022. Microbial detoxification of lignocellulosic biomass
930 hydrolysates: Biochemical and molecular aspects, challenges, exploits and future
931 perspectives. Frontiers in Bioengineering and Biotechnology 10:1061667.
932 76. Jönsson LJ, Martín C. 2016. Pretreatment of lignocellulose: formation of inhibitory by-
933 products and strategies for minimizing their effects. Bioresource technology 199:103-112.
934 77. Luo H, Zheng P, Bilal M, Xie F, Zeng Q, Zhu C, Yang R, Wang Z. 2020. Efficient bio-
935 butanol production from lignocellulosic waste by elucidating the mechanisms of Clostridium
936 acetobutylicum response to phenolic inhibitors. Science of the total environment
937 710:136399.
938 78. Jayakody LN, Turner TL, Yun EJ, Kong II, Liu J-J, Jin Y-S. 2018. Expression of Gre2p
939 improves tolerance of engineered xylose-fermenting Saccharomyces cerevisiae to
940 glycolaldehyde under xylose metabolism. Applied microbiology and biotechnology
941 102:8121-8133.
942 79. Bonn G, Bobleter O. 1984. HPLC-analyses of plant biomass hydrolysis and fermentation
943 solutions. Chromatographia 18:445-448.
944 80. Chandrangsu P, Dusi R, Hamilton CJ, Helmann JD. 2014. Methylglyoxal resistance in B
945 acillus subtilis: contributions of bacillithiol-dependent and independent pathways. Molecular
946 microbiology 91:706-715.
947 81. Walker C, Dien B, Giannone RJ, Slininger P, Thompson SR, Trinh CT, Tullman-Ercek D.
948 2021. Exploring Proteomes of Robust Yarrowia lipolytica Isolates Cultivated in Biomass

949 Hydrolysate Reveals Key Processes Impacting Mixed Sugar Utilization, Lipid
950 Accumulation, and Degradation. mSystems 6:e00443-21.
951 82. Walker C, Mortensen Jr M, Poudel B, Cotter C, Myers R, Okekeogbu IO, Ryu S, Khomami
952 B, Giannone RJ, Laursen S. 2023. Proteomes reveal metabolic capabilities of Yarrowia
953 lipolytica for biological upcycling of polyethylene into high-value chemicals. Msystems
954 8:e00741-23.
955 83. Eid J, Fehr A, Gray J, Luong K, Lyle J, Otto G, Peluso P, Rank D, Baybayan P, Bettman B.
956 2009. Real-time DNA sequencing from single polymerase molecules. Science 323:133-138.
957 84. Kolmogorov M, Yuan J, Lin Y, Pevzner PA. 2019. Assembly of long, error-prone reads
958 using repeat graphs. Nature Biotechnology 37:540-546.
959 85. Chin C-S, Alexander DH, Marks P, Klammer AA, Drake J, Heiner C, Clum A, Copeland A,
960 Huddleston J, Eichler EE. 2013. Nonhybrid, finished microbial genome assemblies from
961 long-read SMRT sequencing data. Nature methods 10:563-569.
962 86. Parks DH, Imelfort M, Skennerton CT, Hugenholtz P, Tyson GW. 2015. CheckM: assessing
963 the quality of microbial genomes recovered from isolates, single cells, and metagenomes.
964 Genome research 25:1043-1055.
965 87. Russel J, Pinilla-Redondo R, Mayo-Muñoz D, Shah SA, Sørensen SJ. 2020.
966 CRISPRCasTyper: automated identification, annotation, and classification of CRISPR-Cas
967 loci. The CRISPR journal 3:462-469.
968 88. Galata V, Fehlmann T, Backes C, Keller A. 2019. PLSDB: a resource of complete bacterial
969 plasmids. Nucleic acids research 47:D195-D202.

970 89. Zhang R, Mirdita M, Levy Karin E, Norroy C, Galiez C, Söding J. 2021. SpacePHARER:
971 sensitive identification of phages from CRISPR spacers in prokaryotic hosts. Bioinformatics
972 37:3364-3366.
973 90. Grant JR, Enns E, Marinier E, Mandal A, Herman EK, Chen C-y, Graham M, Van Domselaar
974 G, Stothard P. 2023. Proksee: in-depth characterization and visualization of bacterial
975 genomes. Nucleic Acids Research:gkad326.
976 91. Tatusova T, DiCuccio M, Badretdin A, Chetvernin V, Ciufo S, Li W. 2013. Prokaryotic
977 genome annotation pipeline, The NCBI Handbook [Internet] 2nd edition. National Center
978 for Biotechnology Information (US).
979 92. Treangen TJ, Ondov BD, Koren S, Phillippy AM. 2014. The Harvest suite for rapid core-
980 genome alignment and visualization of thousands of intraspecific microbial genomes.
981 Genome biology 15:1-15.
982 93. Croucher NJ, Page AJ, Connor TR, Delaney AJ, Keane JA, Bentley SD, Parkhill J, Harris
983 SR. 2014. Rapid phylogenetic analysis of large samples of recombinant bacterial whole
984 genome sequences using Gubbins. Nucleic Acids Research 43:e15-e15.
985 94. Polpitiya AD, Qian W-J, Jaitly N, Petyuk VA, Adkins JN, Camp DG, II, Anderson GA,
986 Smith RD. 2008. DAnTE: a statistical tool for quantitative analysis of -omics data.
987 Bioinformatics 24:1556-1558.
988 95. Tyanova S, Temu T, Sinitcyn P, Carlson A, Hein MY, Geiger T, Mann M, Cox J. 2016. The
989 Perseus computational platform for comprehensive analysis of (prote) omics data. Nature
990 methods 13:731.
991 96. Zhang X, Smits AH, Van Tilburg GB, Ovaa H, Huber W, Vermeulen M. 2018. Proteome-
992 wide identification of ubiquitin interactions using UbIA-MS. Nature protocols 13:530-550.